AD-A174 279

AFWAL-TR-86-4115

THE VARIABILITY OF FATIGUE CRACK GROWTH LIFE OF ALUMINUM CASTING ALLOY A357-T6

J. D. TIRPAK, CAPT, USAF
Materials Engineering Branch
Systems Support Division

1 July 1986

DTIC
ELECTE
NOV 20 1986
S D
E

Final Report for Period April 1984 - May 1985

DTIC FILE COPY

Approved for public release; distribution unlimited.

MATERIALS LABORATORY
AIR FORCE WRIGHT AERONAUTICAL LABORATORIES
AIR FORCE SYSTEMS COMMAND
WRIGHT-PATTERSON AFB, OHIO 45433-6533

86 11 19 045

NOTICE

When Government drawings, specifications, or other data are used for any purpose other than in connection with a definitely related Government procurement operation, the United States Government thereby incurs no responsibility nor any obligation whatsoever; and the fact that the government may have formulated, furnished, or in any way supplied the said drawings, specifications, or other data, is not to be regarded by implication or otherwise as in any manner licensing the holder or any other person or corporation, or conveying any rights or permission to manufacture use, or sell any patented invention that may in any way be related thereto.

This report has been reviewed by the Office of Public Affairs (ASD/PA) and is releasable to the National Technical Information Service (NTIS). At NTIS, it will be available to the general public, including foreign nations.

This technical report has been reviewed and is approved for publication.

JON D. TIRPAK, CAPTAIN, USAF
Engineering & Design Data
Materials Engineering Branch
Systems Support Division

CLAYTON L. HARMSWORTH, Tech Mgr
Engineering & Design Data
Materials Engineering Branch
Systems Support Division

FOR THE COMMANDER:

THEODORE J. REINHART, Chief
Materials Engineering Branch
Systems Support Division
Materials Laboratory

"If your address has changed, if you wish to be removed from our mailing list, or if the addressee is no longer employed by your organization please notify AFWAL/MLSE, Wright-Patterson AFB OH 45433-6533 to help us maintain a current mailing list."

Copies of this report should not be returned unless return is required by security considerations, contractual obligations, or notice on a specific document.

DISCLAIMER NOTICE

THIS DOCUMENT IS BEST QUALITY PRACTICABLE. THE COPY FURNISHED TO DTIC CONTAINED A SIGNIFICANT NUMBER OF PAGES WHICH DO NOT REPRODUCE LEGIBLY.

UNCLASSIFIED

SECURITY CLASSIFICATION OF THIS PAGE

REPORT DOCUMENTATION PAGE

1a. REPORT SECURITY CLASSIFICATION UNCLASSIFIED	1b. RESTRICTIVE MARKINGS
2a. SECURITY CLASSIFICATION AUTHORITY	3. DISTRIBUTION/AVAILABILITY OF REPORT Approved for public release; distribution unlimited.
2b. DECLASSIFICATION/DOWNGRADING SCHEDULE	
4. PERFORMING ORGANIZATION REPORT NUMBER(S) AFWAL-TR-86-4115	5. MONITORING ORGANIZATION REPORT NUMBER(S)
6a. NAME OF PERFORMING ORGANIZATION AFWAL Materials Laboratory 6b. OFFICE SYMBOL (If applicable) AFWAL/MLSE	7a. NAME OF MONITORING ORGANIZATION
6c. ADDRESS (City, State and ZIP Code) AFWAL/MLSE Wright-Patterson AFB OH 45433-6533	7b. ADDRESS (City, State and ZIP Code)
8a. NAME OF FUNDING/SPONSORING ORGANIZATION 8b. OFFICE SYMBOL (If applicable)	9. PROCUREMENT INSTRUMENT IDENTIFICATION NUMBER
8c. ADDRESS (City, State and ZIP Code)	10. SOURCE OF FUNDING NOS.

PROGRAM ELEMENT NO.	PROJECT NO.	TASK NO.	WORK UNIT NO
62102F	2418	07	03

11. TITLE (Include Security Classification)
See Block 16

12. PERSONAL AUTHOR(S)
J.D. Tirpak, Capt, USAF

13a. TYPE OF REPORT	13b. TIME COVERED	14. DATE OF REPORT (Yr., Mo., Day)	15. PAGE COUNT
Final	FROM Apr 84 TO May 85	July 1986	69

16. SUPPLEMENTARY NOTATION

The Variability of Fatigue Crack Growth Life of Aluminum Casting Alloy A357-T6

17. COSATI CODES		
FIELD	GROUP	SUB. GR.
11	06	

18. SUBJECT TERMS (Continue on reverse if necessary and identify by block number)
Fatigue Crack Growth
Cast Aluminum
A357-T6
Life Variability
Metallography
Fractography

19. ABSTRACT (Continue on reverse if necessary and identify by block number)

This investigation considers the variability of fatigue crack growth (FCG) life of A357-T6. The life variability for this cast aluminum alloy is greater than the variability of 2024-T3, a wrought aluminum alloy. Dendrite arm spacing (DAS), dendrite cell size (DCS), porosity and silicon particle aspect ratios are measured to characterize the test specimens. Metallographic and fractographic analyses are performed to aid potential correlations between microstructure and discontinuities and fatigue behavior. Several recommendations are made for future efforts.

20. DISTRIBUTION/AVAILABILITY OF ABSTRACT UNCLASSIFIED/UNLIMITED ☒ SAME AS RPT ☐ DTIC USERS ☐	21. ABSTRACT SECURITY CLASSIFICATION UNCLASSIFIED

22a. NAME OF RESPONSIBLE INDIVIDUAL	22b. TELEPHONE NUMBER (Include Area Code)	22c. OFFICE SYMBOL
CAPT J.D. TIRPAK	(513) 255-5063	AFWAL/MLSE

DD FORM 1473, 83 APR EDITION OF 1 JAN 73 IS OBSOLETE.

UNCLASSIFIED

SECURITY CLASSIFICATION OF THIS PAGE

PREFACE

This report was prepared by the Materials Engineering Branch (AFWAL/MLSE), Systems Support Division, Materials Laboratory, Air Force Wright Aeronautical Laboratories, Wright-Patterson Air Force Base, Ohio, under Project 2418, "Aerospace Structural Materials," Task 241807, "Systems Support," Work Unit 24180703, "Engineering and Design Data."

The work herein was performed between April 1982 and May 1985. The report was released in June 1986.

Accession For
NTIS GRA&I ☒
DTIC TAB ☐
Unannounced ☐
Justification
By
Distribution/
Availability Codes
Dist | Avail and/or Special
A-1

QUALITY INSPECTED 1

TABLE OF CONTENTS

SECTION		PAGE
I	INTRODUCTION	1
II	BACKGROUND	2
III	EXPERIMENTAL PROCEDURES	4
	A. Material Selection	4
	B. Fatigue Test Specimen Configuration	8
	C. Fatigue Testing	8
	D. Tensile Testing	11
	E. Post Fracture Evaluation	14
IV	RESULTS AND DATA ANALYSES	15
	A. Crack Growth Data	15
	B. Statistical Analysis of FCG Data	18
	C. Tensile Data	22
	D. Microstructural Results	25
	E. Fractographic Results	33
V	CONCLUSIONS	38
VI	RECOMMENDATIONS	39

LIST OF ILLUSTRATIONS

FIGURE		PAGE
1.	Sketch of bulkhead from which compact tension test specimens were excised.	5
2.	Test specimens: (a) Compact Tension (CT) and (b) Tensile.	9
3.	Overall view of the test stand used to generate FCG data. A-Crack Gage Monitor, B-Amplitude Controller, C-Environmental Cabinet, D-Servo-hydraulic Controller.	12
4.	Close-up view of a specimen in the sealed environmental control cabinet. A-CT specimen with crack gage leads coming off the backside B-Dessicant, C-Temperature and relative humidity detectors.	13
5.	Composite plot of FCG life data obtained from the eight test specimens tested under the same loading conditions.	16
6.	Composite plot of FCGR data from all nine specimens tested. Scatterbands represent limit of data generated in an earlier study.[17]	17
7.	Schematic of how subsets of crack growth intervals were calculated. Group A coefficients of variation were calculated from a_i to a_f. Group B coefficients of variation were calculated from a_i to a_{i+1}. See Table IV for calculated FCG life statistics.	19
8.	Group A FCG life composite plots. (a) a_o = 0.688 inches, (b) a_o = 0.749 inches, (c) a_o = 0.841 inches, (d) a_o = 1.026 inches.	21
9.	Typical Microstructure. Specimen M2, Keller's etch. 100x.	26

LIST OF ILLUSTRATIONS - Continued

FIGURE		PAGE
10.	Graphic display of $\lvert M_A-M_B \rvert$ and $N-\bar{N}$. The specimens with FCG lives much different from the average FCG life had $\lvert M_A-M_B \rvert$ values exceeding 5.0 (L1, M2, S2). The other specimens, with lives nearest the average FCG life, had $\lvert M_A-M_B \rvert$ values of less than 2.3.	29
11.	Crack path morphology at two different delta K levels in specimen L2: (a) 7 ksi-in$^{\frac{1}{2}}$, transdendritic, (b) 18 ksi-in$^{\frac{1}{2}}$, interdendritic. Arrows indicate crack propagation direction, Keller's etch. 100x.	30
12.	Typical shrinkage porosity encountered by crack path. Specimen L2. Arrow indicates crack propogation direction. Keller's etch. 200x.	31
13.	Examples of crack branching, (a) Specimens L2 (125x), (b) Specimen S2 (200x). Arrow indicates crack propagation direction, Keller's etch.	32
14.	Typical macroscopic view of a fracture face. Note faceted appearance of region 1, and the transition of region 1 to region 2, and the ductile appearance of region 2. Arrow indicates crack propagation direction. Approximately 3x.	34
15.	Region 1 fracture features. Note ductility, limited signs of fatigue, and lack of fractured silicon particles, 200x.	34
16.	Localized region of fatigue striations on aluminum matrix. Also, fractured and secondary cracked silicon particle, 2200x.	35
17.	Region 2 fracture face characterized by fractured silicon particles indicating interdendritic nature of fracture, 720x.	35
18.	Shrinkage porosity typical of that scattered throughout the material, 200x.	37

LIST OF TABLES

TABLE		PAGE
I.	Chemical Analysis by Weight Percent	6
II.	Microstructural Data	7
III.	Test Specimen Dimension and Testing Condition Summary	10
IV.	Fatigue Crack Growth Life Statistics	20
V.	Comparison of FCG Life Statistics for Different Alloys	23
VI.	Actual Tensile Properties and Predicted Percent Elongations	24
VII.	Data Relating the Absolute Difference of M_A and M_B to the Absolute Difference of FCG Life and the Average FCG Life	28

ACKNOWLEDGEMENTS

This study would not have been possible without the assistance of several key people. I am grateful for the practical insight which Mr Gerald Petrak provided; the latitude which Mr Clayton Harmsworth allowed; and the technical expertise and guidance which Drs Joseph Gallagher and Alan Berens shared with me.

Also special thanks and credit go to Messrs Donald Woleslagle and Thomas Dusz of the University of Dayton Research Institute for assisting in generating the fatigue and microstructural data; Mr Mark Marsh of Boeing Corporation for performing the Image Analysis; and especially to Misses Sherri Swihart, Connie Herrmann, and Nancy Chambless for their immeasurable patience in dealing with yet another technical report.

To all, many thanks.

SECTION I
INTRODUCTION

The variability of cast aluminum mechanical properties has partly prevented designers from using aluminum castings in fracture critical structural applications. Recently, however, premium quality aluminum casting technology has matured to the point where variability has decreased considerably and sound cast parts can be reproduced with guaranteed tensile properties. Although low variability of casting tensile properties has been demonstrated, the variability of damage tolerant properties such as fatigue crack growth rate (FCGR) or fracture toughness has not been determined.

This report details a program conducted to evaluate the variability of FCGR properties by focusing on fatigue crack growth (FCG) life of a commonly used structural aluminum casting alloy (A357 in the T6 condition).

SECTION II
BACKGROUND

Over the past several years, premium quality aluminum casting technology has attracted considerable attention in the aerospace structures community. This interest was stimulated primarily by the tremendous cost savings which castings offer as compared to structures composed of mechanically fastened wrought products.[1-4] While premium quality casting technology developed, the application of fracture mechanics in airframe design also increased. Although premium quality castings have respectable mechanical properties, they were, for the most part, relegated to non-fracture critical structures. This was due to a variety of reasons such as unfavorable experiences with non-premium quality castings; substantial weight penalties (due to heavier cross-sections and conservative factors of safety); and inferior properties.[5] Many of these reasons were well-founded, but it is believed that premium quality aluminum castings can be applied in fracture critical applications once several major issues are satisfactorily resolved.

One of these issues involves the variability of premium quality casting properties especially fatigue, fatigue crack growth and fracture toughness. With current premium quality casting technology, tensile properties (ultimate and yield strengths and percent elongations) can be controlled, reproduced, predicted and guaranteed in designated areas of the castings with minimal variability. Although this is true with tensile properties, this has not been proven for fatigue, fatigue crack growth or fracture toughness. This stems from the fact that (1) there was little need for this data ("they were...relegated to non-fracture critical structures") and therefore, (2) few data were generated. With this in mind, a program was designed to evaluate the variability of fatigue crack growth life of premium quality aluminum castings.

Some earlier studies addressed the variability of FCG life and FCGR. Shaw and Lemay determined, using different tempers of AISI 4140, that the coefficient of variation (standard deviation/mean) of FCGR at a fixed range of stress intensity factor (delta K) was approximately equal to the variation of FCG life.[6]

For wrought aluminum, Berens et. al. demonstrated that the coefficient of variation for FCG life distributions of an aluminum alloy (2024-T3) ranged from 7.0 to 8.7 percent.[7] The experimental data used were generated by Virkler et. al. in an earlier study which involved evaluating FCG and FCGR data from sixty-eight center cracked panels tested under identical conditions.[8] Berens also calculated coefficients of variation for other alloy systems: for a 10Ni-8Co-1Mo steel the coefficient of variation of life was 6%, while for IN-718 the coefficient of variation of life was 6.6% at 1000°F and 9% at 940°F.[9] Again, the emphasis was placed on wrought products and not cast products.

The main purpose of this program is to compare the variability of FCG life distributions for premium quality aluminum castings to that of wrought aluminum alloys.

SECTION III
EXPERIMENTAL PROCEDURES
A. Material Selection

Aluminum casting alloy A357 was selected in this study for several reasons. First, A357 is one of the most commonly used cast alloys in aerospace applications due to its excellent castability and moderate mechanical properties. Second, although A357's static properties (ultimate, yield, and ductility) have been well documented, little has been done to relate damage tolerant properties (FCG, FCGR, K_{IC}, etc.) to microstructural features. Third, the material was readily available; several fully characterized bulkhead sections from the CAST Program[10] were still in storage.

The material used in this program was excised from a bulkhead shown in Figure 1. Specimens were selected from regions with microstructures containing small, medium, and large dendrite arm spacing; hence, the test specimens were identified with the nomenclature S, M, L.

The bulkhead was heat treated to the T6 condition as follows: (1) solution heat treat at 1010°F for 24 hours, (2) H_2O quench at 160°F with a nine second quench delay, (3) natural age at room temperature for 24 hours, and (4) artificially age at 325°F for eight hours.

A sample of the bulkhead was sectioned to confirm the chemical composition. The composition was within specification except for the slightly high magnesium content as shown in Table I.

Image analysis was performed on the machined compact tension specimens. Dendrite Cell Size (DCS), silicon particle aspect ratio, porosity measurements and ductility predictions were performed on each side of the specimens[11]. In addition, Dendrite Arm Spacing (DAS) measurements were also made[12]. (Table II)

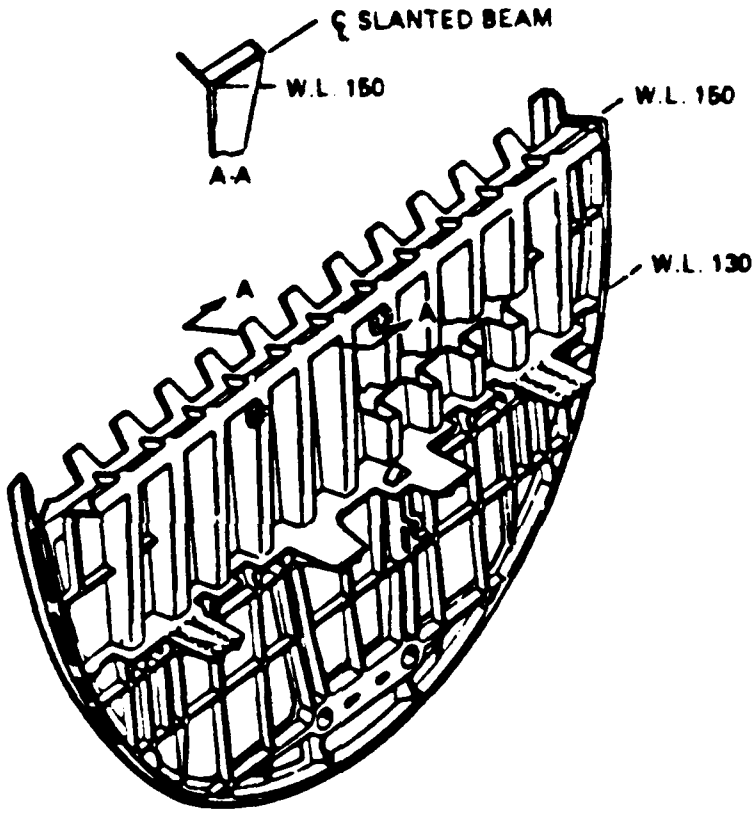

Figure 1. Sketch of bulkhead from which compact tension test specimens were excised.

TABLE I: Chemical Analysis by Weight Percent

Element	Bulkhead	MIL-A-21180C Specification
Silicon	6.93	6.5-7.5
Magnesium	0.78	0.40-0.7
Manganese	0.01	0.10 max.
Iron	0.13	0.20 max.
Copper	0.01	0.20 max.
Zinc	0.01	0.10 max.
Titanium	0.12	0.10-0.20
Chromium	0.01	---
Beryllium	0.042	0.04-0.07
Others, each	0.05	0.05 max.
Others, total	0.15	0.15 max.
Aluminum	Balance	Balance

TABLE II: Microstructural Data

	N			AR			P			M			Elongation			DAS		
	A	B	AVG	A	B	AVG	A	B	AVG	A	B	AVG	A	B	AVG	A	B	AVG
S1	30.9	27.0	28.9	1.789	1.851	1.825	0.161	0.068	0.115	24.2	23.7	24.0	5.4	5.2	5.3	16	12	14
S2*	38.6	31.0	34.8	1.825	1.790	1.808	0.055	0.292	0.173	29.1	22.5	25.8	7.8	4.7	6.3	13	14	13.5
S3	31.4	31.8	31.6	1.756	1.742	1.749	0.237	0.440+	0.339	24.0	21.8	22.9	5.3	4.5	4.9	12	13	12.5
M1	30.2	29.9	30.1	1.733	1.756	1.745	0.034	0.032	0.033	28.3	28.7	28.1	7.3	7.1	7.2	16	16	16
M2	33.3	27.7	30.5	1.799	2.053	1.926	1.388+	0.136	0.761	14.1	19.2	16.7	2.5	3.7	3.1	15	15	15
M3*	32.6	28.8	30.7	1.743	1.790	1.767	0.264	0.320	0.292	24.1	21.2	22.7	5.4	4.3	4.9	15	16	16
L1	38.1	36.3	37.2	1.713	1.817	1.765	0.063	0.216+	0.139	30.3	25.1	27.7	8.5	5.8	7.2	13	13	13
L2	35.6	34.2	34.9	1.896	1.808	1.852	0.812	0.980+	0.896	17.5	16.9	17.2	3.3	3.1	3.2	14	13	13.5
L3	37.5	32.2	34.9	1.783	1.907	1.845	0.422	0.149	0.285	23.4	22.3	22.9	5.1	5.0	5.1	16	14	15
	A	B		A	B		A	B		A	B		A	B		A	B	
$\bar{x}$	34.2	31.0		1.782	1.035		0.382	0.293		23.8	22.4		5.6	4.8		14.4	14	
s	3.27	3.03		0.055	0.095		0.449	0.288		5.3	3.4		1.98	1.17		1.51	1.4	
$s/\bar{x}$	0.095	0.098		0.031	0.052		1.18	0.99		0.22	0.15		0.35	0.24		0.10	0.10	

* Used in calculating averages but not in statistical analysis of FCG data
\+ gross porosity skewed data

N = Number of cells per 0.0001 $inch^2$
AR = Silicon Particle Aspect Ratio
P = % Porosity
M = Microstructural Parameter = $14.72N^{1/2} - 18.71N^{1/2}/AR + 159.7/AR - 14.3P^{1/2} - 82.8$
Elongation = $10^{((M-1.89)/30.48)}$
DAS = Dendrite Arm Spacing, 0.0001 inches

A = Side 1 of specimen
B = Side 2 of specimen

$\bar{x}$ = mean
s = standard deviation
$s/\bar{x}$ = coefficient of variation

B. Fatigue Test Specimen Configuration

The Compact Tension (CT) fatigue specimen configuration shown in Figure 2(a) was used in this study. Nine specimens were machined to the following dimensions: B = 0.120 ± 0.002 in, and W = 2.000 ± 0.001 in. Once measured on a toolmakers scope, a Fractomat foil crack gage was mounted on one side of the specimen.

The K solution for the compact tension specimen is as follows:

$$K = (P x (2 + alpha))/(B \times W^{\frac{1}{2}} \times (1 - alpha)^{3/2}) x$$
$$(0.866 + 4.64 \times alpha - 13.32 \times alpha^2 + 14.72 \times alpha^3 - 5.6\ alpha^4)$$

where K = stress intensity
P = load applied
alpha = a/W
B = specimen thickness
W = specimen width
a = crack length.

C. Fatigue Testing

Each of the nine specimens were subjected to the same loading conditions. Loads were applied sinusoidally at 25 Hz using a 2.2 kip MTS servohydraulic axial fatigue machine. Loads of Pmax = 225 lbf and Pmin = 45 lbf (R ratio=0.2) were controlled within 0.5%. Test conditions are listed in Table III. Crack length was constantly monitored with the foil gages and were accurate to one mil. At 0.015 inch intervals, the computer printed the crack length, cycles and approximated the crack growth rate and delta K values. Past experience has proven this system to be highly reliable, precise and fast.[13-14] The best features of the system are the elimination of human error and the ability to run uninterrupted tests.

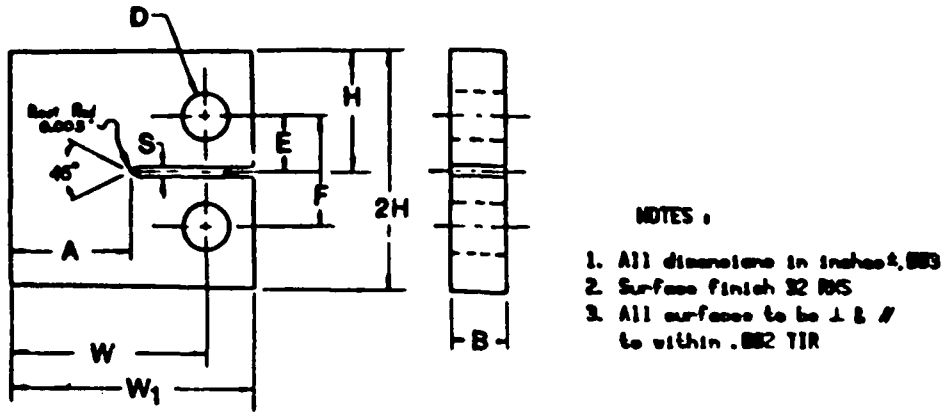

B	A	W	W_1	S	E	F	H	D
0.120	1.35	2.000	2.500	0.096	0.55	1.10	1.200	0.500

(a)

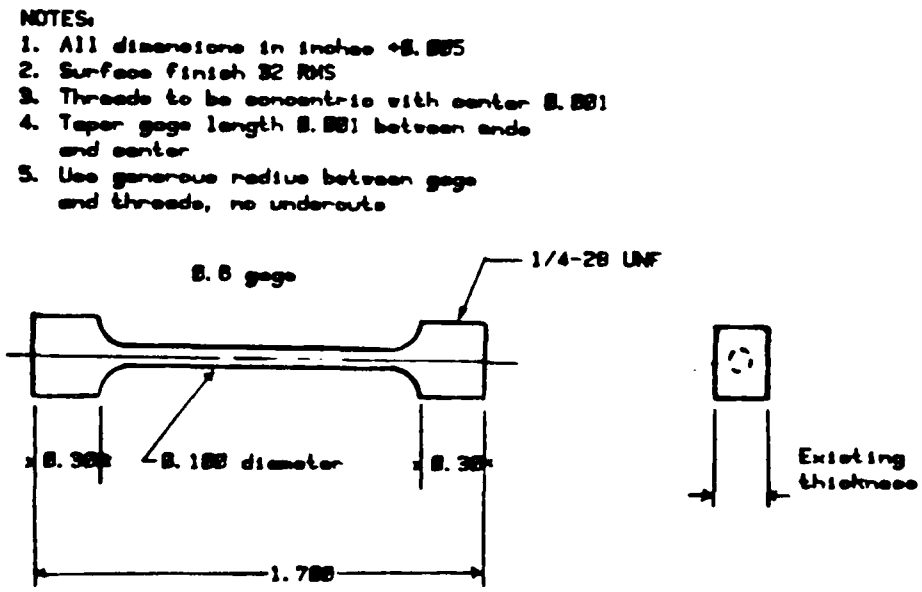

(b)

Figure 2. Test specimens: (a) Compact Tension (CT) and (b) Tensile.

TABLE III: Test Specimen Dimension and Testing Condition Summary

Specimen	Thickness (B, in)	Width (W, in)	a_o (in)	a_f (in)	P_{max} (kips)	P_{min} (kips)
S1	0.1220	2.0004	0.672	1.395	0.225	0.045
S2	0.1218	1.9985	0.683	1.373	0.225	0.045
S3	0.1210	2.0001	0.657	1.317	0.225	0.045
M1	0.1214	2.0000	0.671	1.368	0.225	0.045
M2	0.1220	2.0000	0.673	1.383	0.225	0.045
M3*	0.1220	2.0007	0.690	1.253	0.300	0.060
L1	0.1200	2.0010	0.677	1.327	0.225	0.045
L2	0.1210	1.9996	0.671	1.345	0.225	0.045
L3	0.1200	1.9905	0.666	1.372	0.225	0.045

Notes:

- Sinusoidal waveform was applied at 25 Hz
- R = 0.2
- For statistical analysis, a_o = 0.688 inches and a_f = 1.302
- Fatigue precracking was accomplished by stepping down loads.
- Fatigue testing was conducted in accordance with ASTM Standard E647

*M3 overloaded during precracking; subsequently tested at higher loads.

Figure 3 illustrates the test system employed for generating the fatigue crack growth data. Not shown in this photograph are the HP 9825B Desk Top Computer and 6490B Multi Programmer which controlled the test and acquired the crack length and cycle count automatically.

A close up view of the specimen under fatigue loading is shown in Figure 4. The sealed plastic chamber minimized temperature excursions and maintained relative humidity at less than 5%. Although thin specimen buckling was anticipated, it did not occur. This was attributed to the grip design and alignment and the low loads applied. During precracking the ungaged side was monitored. Once precracking was completed, crack lengths were monitored by the foil gage on the opposite side. Data were taken at crack growth rates above 2×10^{-7} inch/cycle (Stages II and III) and covered three decades of crack growth. Time constraints prevented testing at rates below 2×10^{-7} inch/cycle (Stage I, the threshold region). Overall, precracking and testing were conducted in accordance with ASTM standards.[15]

During the precracking of specimen M3, the specimen was accidently overloaded and the crack tip severely blunted at 0.670 inches. The blunting was so severe that it was not possible to include this specimen with the others in the FCG life analysis. So, the load was increased to grow the crack through the overloaded region and to obtain FCGR data which could be compared with the other FCGR data.

D. Tensile Testing

Tensile tests using specimens machined from broken CT specimens were conducted to verify the elongation predictions. Tests were conducted on a 10 kip Instron tensile test machine.[16] The compact tension specimen thickness (B) and width (W) prevented the use of standard tensile specimens so the sub-size specimen shown in Figure 2(b) was designed.

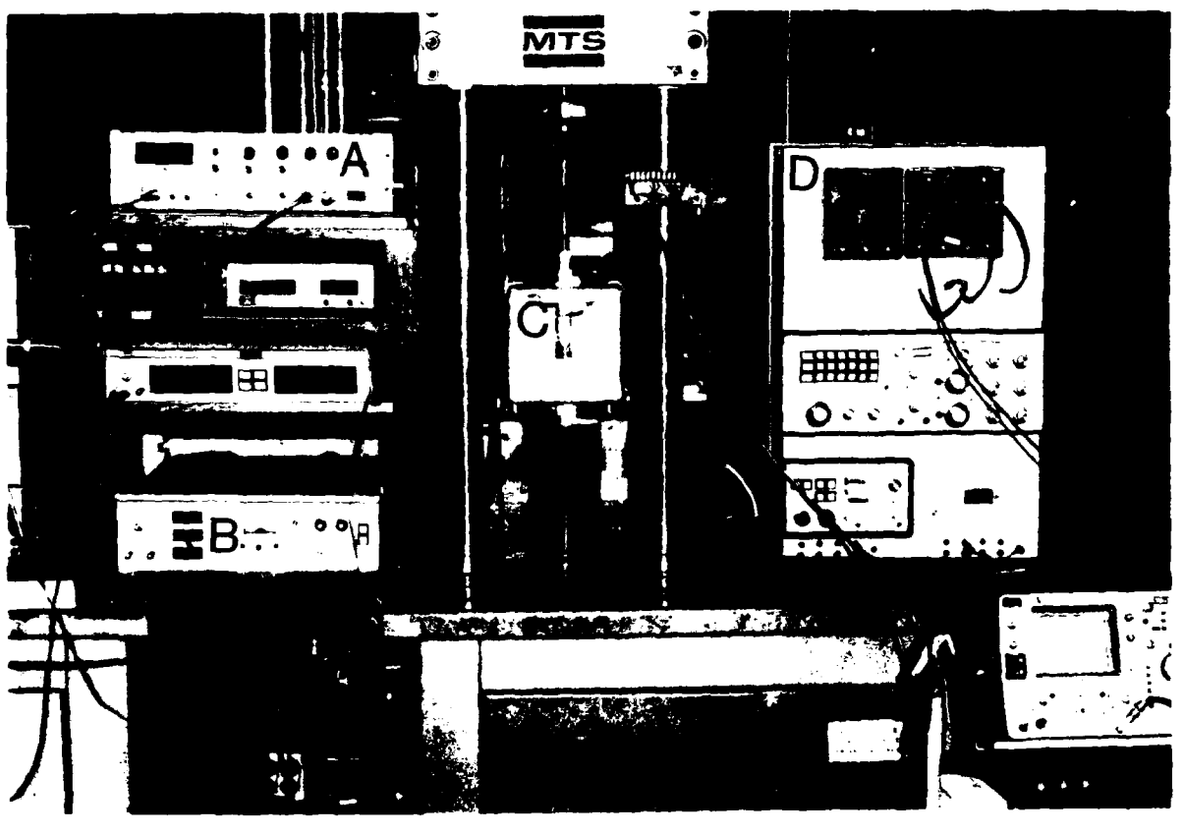

Figure 3. Overall view of the test stand used to generate FCG data. A-Crack gage monitor, B-Amplitude Controller, C-Environmental Cabinet, D-Servohydraulic controller.

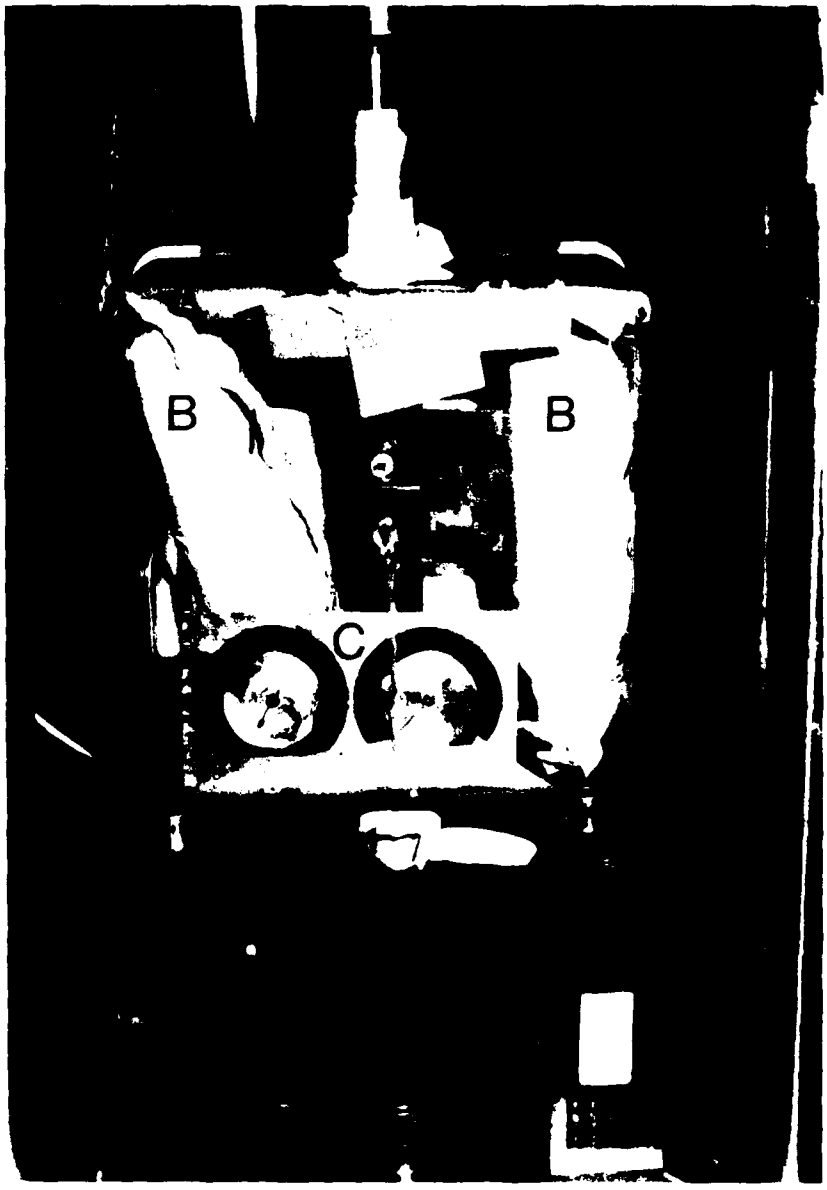

Figure 4. Close up view of a specimen in the sealed environmental control cabinet. A-CT specimen with crack gage leads coming off the backside, B-Dessicant, C-Temperature and relative humidity detectors.

F. Post Fracture Evaluation

Selected halves of broken specimens were carefully sectioned, mounted, ground, polished, and etched to reveal the microstructure and crack path morphology. By including the notch tip, it was possible to evaluate the crack path from the notch, through the fatigue zone, to the overload region. The notch served as a landmark for calculating crack length and for comparing the features to crack length, FCGR, and delta K. Metallographic analysis was performed on a Zeiss metallograph.

Fracture faces were also examined macroscopically and microscopically with light and electron optics. Macroscopic light optics magnifications ranged from 1x to 70x. A Jeol 35CFX Scanning Electron Microscope was used for higher magnifications of 70x to 5000x.

Initially, this program was designed to reveal relationships between cast microstructural features and fatigue crack growth lives. When the material was selected, it was believed that a broad range of microstructural features was obtainable. Unfortunately, after the image analysis data were generated, it was discovered that the range of dendrite arm spacing, dendrite cell size, silicon particle aspect ratio, and porosity displayed a smaller range than anticipated. The observed variability in microstructure limited the possibility of drawing solid conclusions at program completion. With this in mind, the program was redirected to evaluate the variability of fatigue crack growth lives using the prepared specimens and the data generated on these specimens.

SECTION IV
RESULTS AND DATA ANALYSES
A. Crack Growth Data

The FCG data are compared in Figure 5 based on a common initial crack length (a_0) of 0.688 inches. For some of the specimens, the cycle count at a_0 was obtained through interpolation. Figure 5 does not include the overloaded specimen M3 because it was tested at higher loads than the other specimens. As shown in Figure 5, specimen S2 had the longest life of the eight specimens, while specimens M2 and L1 had the shortest lives. There were five specimens which had similar FCG lives.

The FCGR data for each of the nine specimens were also tabulated and individually plotted in the Appendix. Figure 6 is a comparison plot of the FCGR data from all specimens and the scatterband associated with data generated in an another study.[17] Good agreement exist between the results of individual specimens except for specimen S2. Specimen S2 exhibited a substantially different trend and a much slower crack growth rate than any of the other eight specimens tested in this program as well as the specimens tested previously. This type of behavior is extremely unusual.

Since S2 had an unusual crack growth rate, it was not included in the following statistical analysis for two possible reasons. First, it is believed that some piece of test instrumentation may have been improperly calibrated for this test (it was the first test conducted), thereby leading to erroneous data. Second, its microstructure could have been significantly different than the other specimens. The data in Table II indicates there was no significant difference. Therefore, it was concluded that the test instrumentation was improperly calibrated.

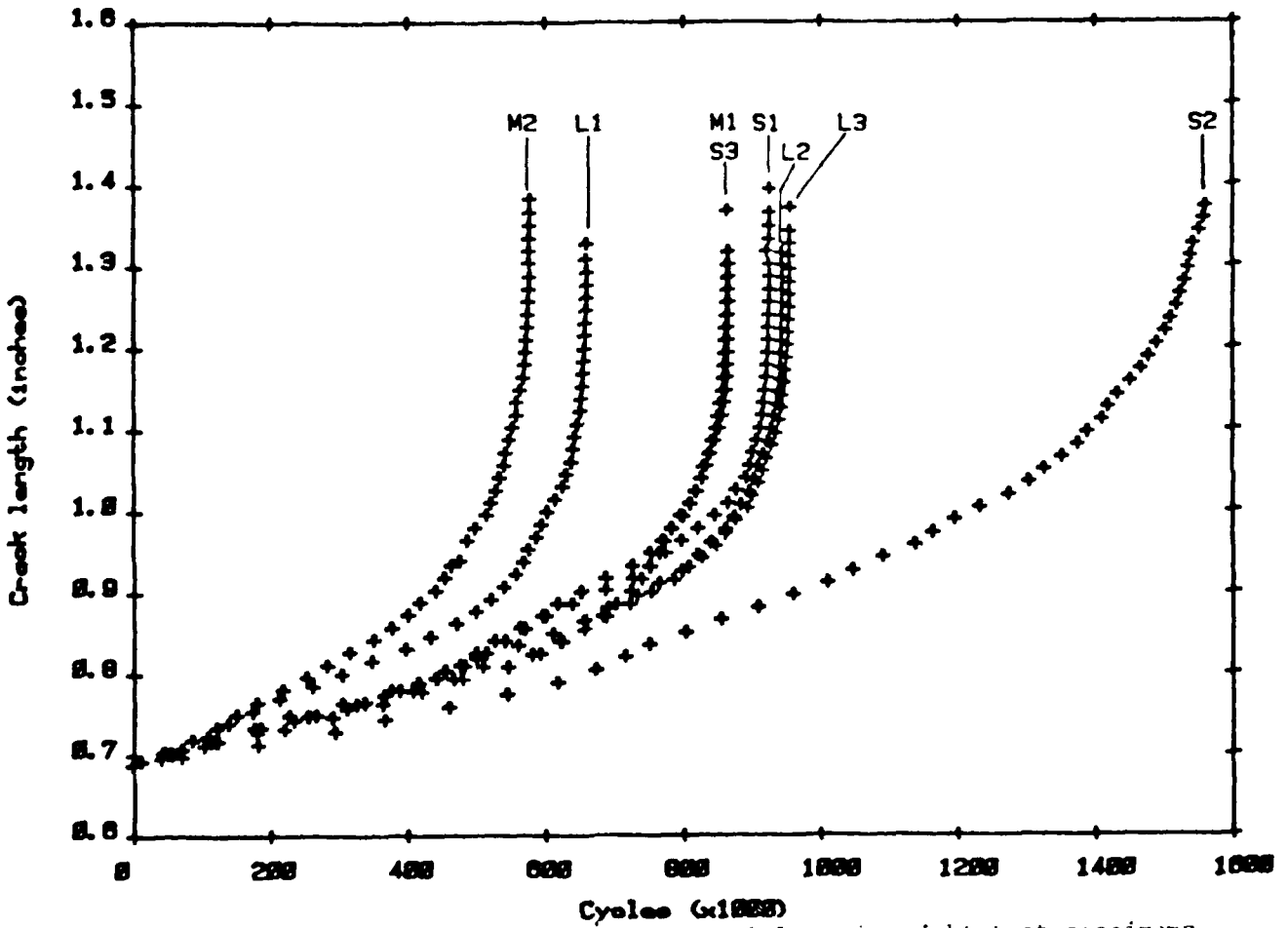

Figure 5. Composite plot of FCG life data obtained from the eight test specimens tested under the same loading conditions.

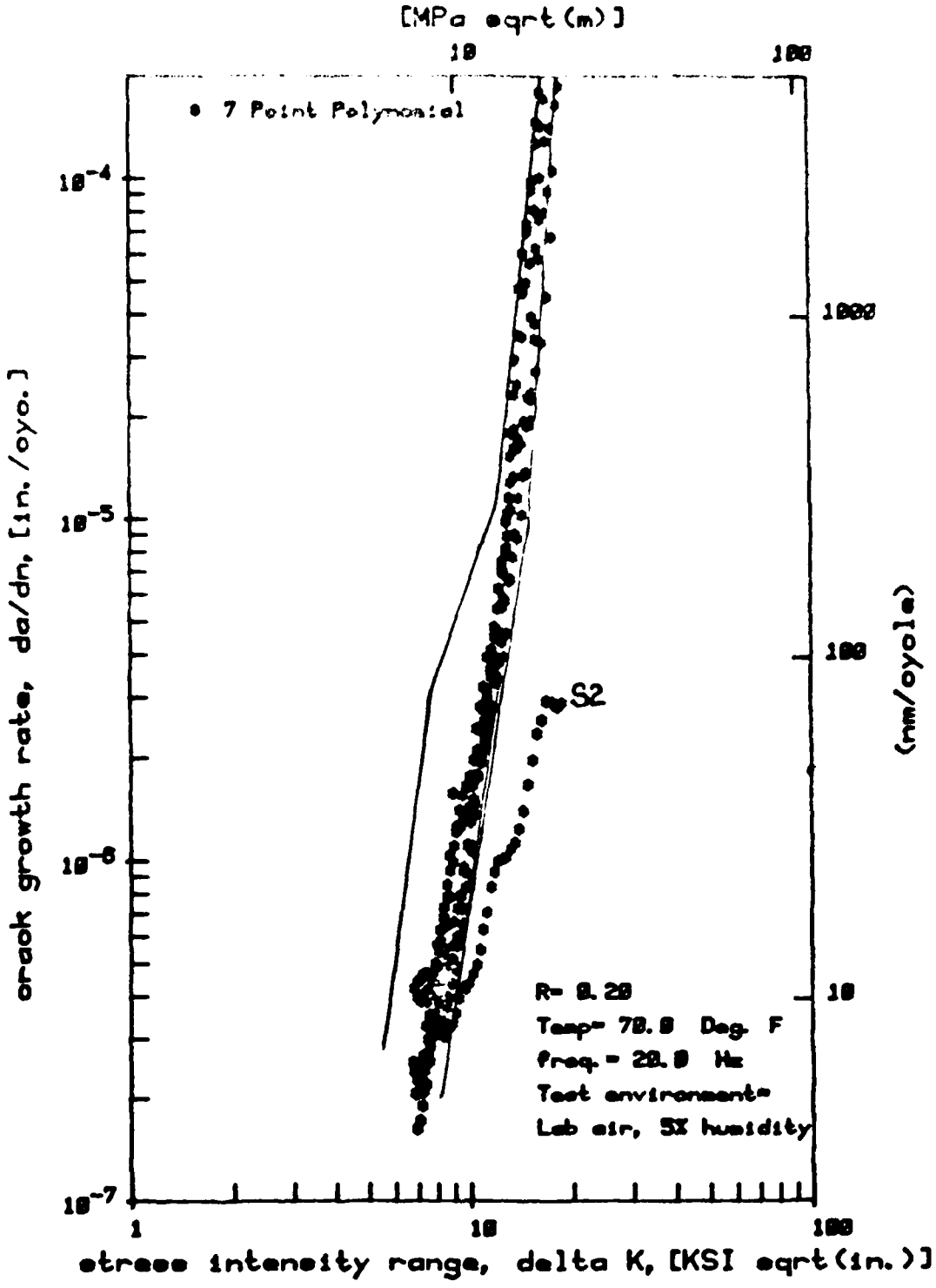

Figure 6. Composite plot of FCGR data from all nine specimens tested. Scatterbands represent limit of data generated in an earlier study.[17]

B. Statistical Analysis of FCG Data

Since only a limited amount of data was available for statistical analysis, it was decided that only basic statistical calculations (mean, standard deviation, and coefficient of variation) would be made.

Figure 7 illustrates the intervals over which the coefficient of variation of FCG life was calculated. Fatigue life statistics were calculated from a_0 = 0.688 inches to a_f = 1.302 inches at 0.092 inch intervals. Two groups of statistics were calculated and tabulated in Table IV. Group A statistics were described as a_i to a_f. For example, the first interval ranged from 0.688 inches to 1.302 inches. The average number of cycles to grow from 0.688 inches to 1.302 inches was 828,190 cycles, and the standard deviation was 149,030 cycles. The coefficient of variation was 0.18 or 18%. The second interval ranged from 0.749 inches to 1.302 inches as shown in Figure 8(b). The average life was 595,270 cycles with a standard deviation of 95,920 cycles, and a coefficient of variation of 16%. Group B statistics were described as a_i to a_{i+1}. For example, the first interval ranged from 0.688 to 0.749 inches, while the second interval ranged from 0.749 to 0.841 inches.

Table IV lists the variability of FCG lives. The least coefficient of variation of 9% occurred when the crack grew from 1.026 to 1.302 inches (Figure 8(d)). The most variability (57%) occurred when the crack became unstable just before fracture. The high 57% variability is also attributed to the few number of cycles that the crack grew during that interval. Then, by the very definition of coefficient of variation (standard deviation/mean), the coefficient of variation for this interval was high.

If the S2 FCG life data were included in the statistical calculations, the coefficient of variation would be even greater. For example, for the interval a_0 = 0.688 inches to a_f = 1.302 inches the

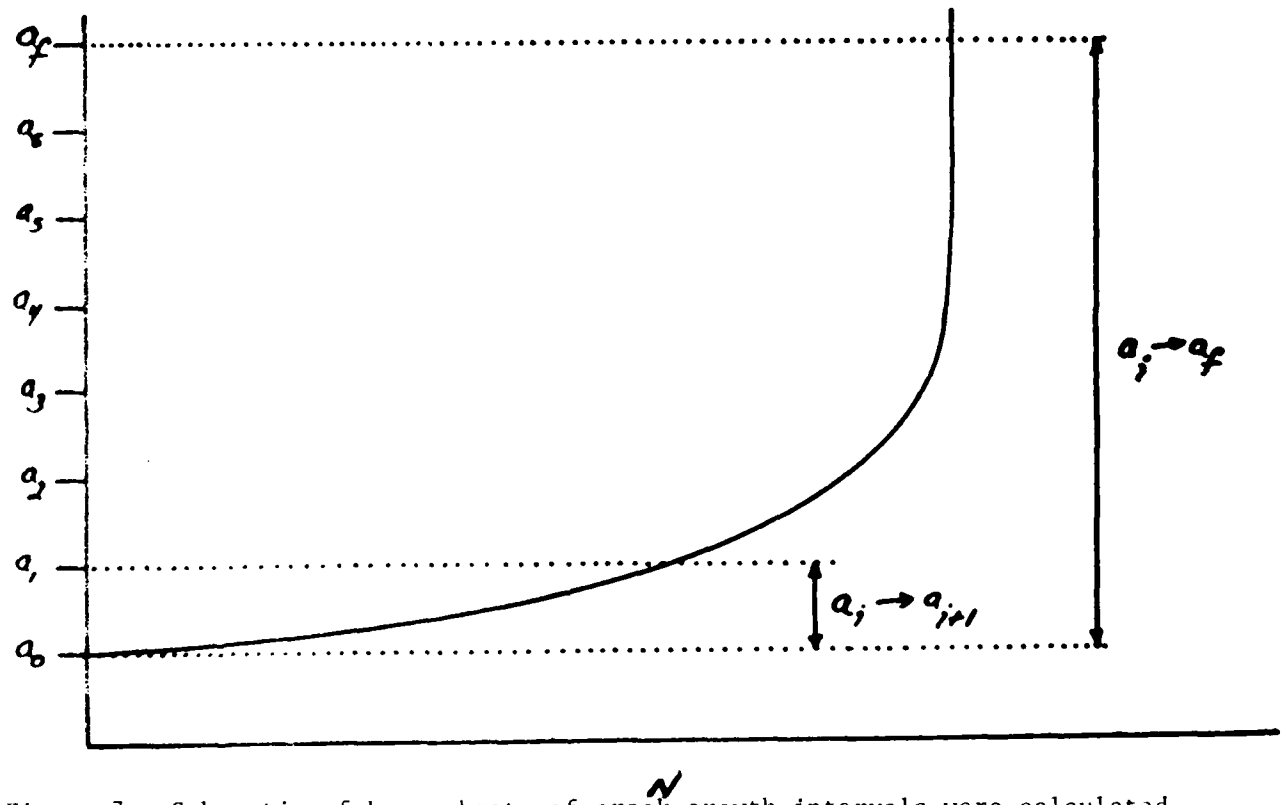

Figure 7. Schematic of how subsets of crack growth intervals were calculated. Group A coefficients of variation were calculated from a_i to a_f. Group B coefficients of variation were calculated from a_i to a_{i+1}. See Table IV for calculated FCG life statistics.

TABLE IV: Fatigue Crack Growth Life Statistics

Group A: $a_i \rightarrow a_f$

a_i (inches)	a_f (inches)	Mean Life (10^3 cycles)	Standard Deviation of Life (10^3 cycles)	C.O.V.
0.688	1.302	828.19	143.03	0.18
0.749	1.302	595.27	95.92	0.16
0.841	1.302	303.63	69.84	0.23
0.933	1.302	131.22	26.70	0.20
1.026	1.302	46.83	4.32	0.09
1.118	1.302	12.75	3.43	0.26
1.210	1.302	2.21	1.26	0.57

Group B: $a_i \rightarrow a_{i+1}$

a_i (inches)	a_{i+1} (inches)	Mean Life (10^3 cycles)	Standard Deviation of Life (10^3 cycles)	C.O.V.
0.688	0.749	232.90	56.25	0.24
0.749	0.841	290.47	55.19	0.19
0.841	0.933	172.32	45.20	0.26
0.933	1.026	84.38	23.61	0.28
1.026	1.118	34.04	4.55	0.13
1.118	1.210	10.54	2.40	0.23
1.210	1.302	2.21	1.26	0.57

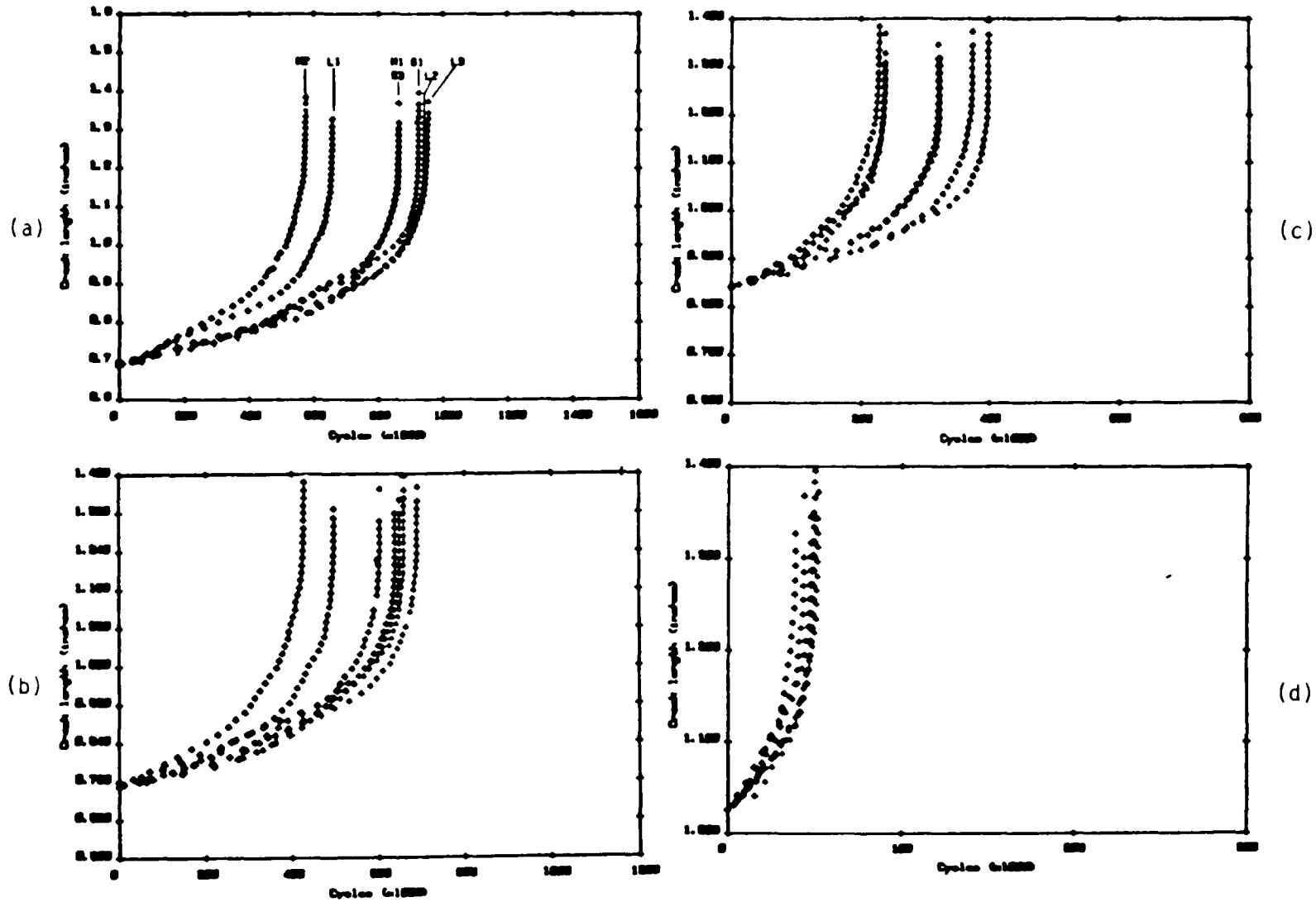

Figure 8. Group A FCG life composite plots. (a) a_0 = 0.6[illegible] inches, (b) a_0 = 0.749 inches, (c) a_0 = 0.841 inches, (d) a_0 = 1.026 inches.

coefficient of variation without specimen S2 is 18% (See Table IV), while if S2 were included the coefficient of variation is 30.3%.

Table V lists FCG life statistics for various alloys. From this table it is obvious that cast A357-T6 has more variability in FCG life than the wrought materials shown.

Considerable variability was expected due to the coarse microstructure and casting discontinuities. When the cracks are small, the coarse, heterogenous microstructure results in various crack growth lives - some short, some long. Similarly, the nonuniform microstructure affects the variability of FCG life and FCGR behavior when the crack approaches the length of instability and final overload fracture. Substantial property variability was also noticed in a study of casting fracture toughness.[18]

C. Tensile Data

The measured tensile properties and predicted elongations were compiled in Table VI. The specimens were listed from shortest to longest FCG life. The data for specimen M3, the overloaded specimen, were included for completeness.

The average ultimate and yield strengths were very close to the strengths expected of A357-T6. Of particular interest was the low coefficient of variation of the strengths: 3.1% for ultimate and 2.8% for yield.

Unlike the strength measurements, both the predicted and actual ductilities (percent elongations) varied considerably; for the predicted elongations, side A measured 35% coefficient of variation while side B measured 46% coefficient of variation, and for the actual elongations, a 49% coefficent of variation was calculated.

TABLE V: Comparison of FCG Life Statistics for Different Alloys

Material	Average C.O.V.	Range of C.O.V.	Reference
A357-T6	0.27	0.13 to 0.57	This Study Group B
2024-T3	0.079	0.07 to 0.085	Ref 7
10 Ni-8Co-1Mo	0.06	0.06	Ref 9
IN 718 @ 940°F	0.09	0.09	Ref 9
IN 718 @ 1000°F	0.066	0.066	Ref 9

TABLE VI: Actual Tensile Properties and Predicted Percent Elongations

Specimens By Life (short to long)	Ultimate Tensile Strength (ksi)	Yield Tensile Strength (ksi, 0.2% offset)	Measured Elongation (%, 0.5" gage)	Predicted Elongation (side A%, side B% avg)		
M2	47.6	42.9	2.2	2.5	3.7	3.1
L1	50.6	45.7	3.4	8.5	5.8	7.2
M1	50.6	44.6	3.0	7.3	7.1	7.2
S3	50.6	42.7	4.9	5.3	4.5	4.9
S1	51.2	43.3	6.2	5.4	5.2	5.3
L2	47.6	42.3	1.8	3.3	3.1	3.2
L3	48.8	43.8	8.5	5.1	5.0	5.1
S2	50.0	42.1	4.2	7.8	4.7	6.3
M3	51.8	44.5	4.1	5.4	4.3	4.6
$\bar{x}$	49.9	43.5	4.3	5.6	4.82	--
s	1.523	1.202	2.086	1.983	0.196	--
$s/\bar{x}$	0.031	0.028	0.49	0.35	0.46	--

Since the tensile specimens were subsize and not located exactly where the image analysis was performed, some of the differences between predicted and actual elongations were anticipated. It is most disturbing, however, that for the predictions made, which predicted value does the quality assurance engineer believe? Which is most accurate, side A or side B? For instance, in Specimen L1, is side A acceptable at 5.8% elongation or is side B acceptable at 8.5% elongation?

Although these questions are posed, the tensile data as a whole is not necessarily precise; it serves to further characterize the material tested under fatigue.

D. Microstructural Results

Upon solidification, the basic microstructure of A357 takes the form shown in Figure 9. This microstructure consists of a dendritic aluminum matrix outlined by silicon eutectic particles. Subsequent solutionizing, quenching, and artificial aging refine the microstructure further and increase tensile strength. Solutionizing slightly homogenizes the microstructure and spheroidizes the silicon particles. During aging, Mg_2Si precipitates form in the matrix; these are primarily strengthening agents while the eutectic silicon particles offer no strengthening. The silicon eutectic enables molten fluidity of the alloy. The material also contains inclusions and gas shrinkage porosity. Since the basic microstructure has been studied extensively, the emphasis of this effort was placed on correlating the microstructural features and discontinuities to FCG life and FCGR behavior.

The microstructural data in Table II were compared to the FCG life data. Unfortunately, no conclusive correlations could be drawn due to the narrow range of microstructural variability. While analyzing the data, it was noticed that specimens M2, L1 and S2 possessed the greatest side-to-side differences in the metallurgical parameter M. In other

Figure 9. Typical Microstructure. Specimen M2, Keller's etch. 100x

words for specimen M2, the difference between side A and side B measurements was 5.1 while specimen S3 measurements differed by 2.2. The FCG life and metallurgical parameter M data illustrating this observation are tabulated in Table VII and shown graphically in Figure 10. Test specimens S1, S3, M1, L2, and L3, which clustered around the average FCG life, had the lowest values of $|M_A-M_B|$. Specimens S2, L1, and M2 had the highest values of $|M_A-M_B|$ and were either much shorter than the average FCG life (approximately one half) or much longer than the average FCG life (approximately twice). By assuming that the life data from specimen S2 is valid, the metallurgical parameter M is shown to provide a direct measure of variability with respect to average fatigue crack growth life. By deleting the S2 fatigue life, the correlation with M becomes much less pronounced.

Crack path morphologies were also studied in great detail. Analysis showed that in the Paris Law region (Stage II) the crack propagated primarily transdendritically, while in the overload region (Stage III) the crack propagated interdendritically (Figure 11). The transition point (delta K_t is the transition stage III of the FCGR plot) was approximately 12.4 ksi $(in)^{\frac{1}{2}}$ which was in good agreement with data generated earlier.[19]

An effort was made to correlate discontinuities, such as porosity and crack branching, to the acceleration or deceleration of the crack tip (Figures 12-13). This was accomplished by measuring the crack length to a given anomally (porosity or crack branching) and then referring back to the calculated crack growth rate data. Typically, FCGR increased when the crack hit shrinkage porosity and decreased when the crack branched. Although this was generally true, a more precise means of measuring the effects of microstructure, discontinuities and branching should be employed. Perhaps the best method would be to make crack length measurements at shorter intervals, such as 0.005 inch increments instead of 0.015 inch increments.

TABLE VII: Data Relating the Absolute Difference of M_A and M_B to the Absolute Difference of FCG Life and the Average FCG Life

Specimen	$\lvert M_A - M_B \rvert$	N^+	$\lvert N - \bar{N} \rvert$
S1	0.5	926.39	9.48
S2	6.6	1537.98	621.07
S3	2.2	866.6	50.31
M1	0.4	864.51	52.4
M2	5.1	577.82	339.09
M3*	---	---	---
L1	5.2	660.63	256.28
L2	0.6	945.09	28.18
L3	1.1	956.26	39.35
		$\bar{N}$=916.91	

*Not included in this analysis due to different loading conditions.

+Common crack length interval a_o = 0.688 inch to a_f = 1.302 inch.

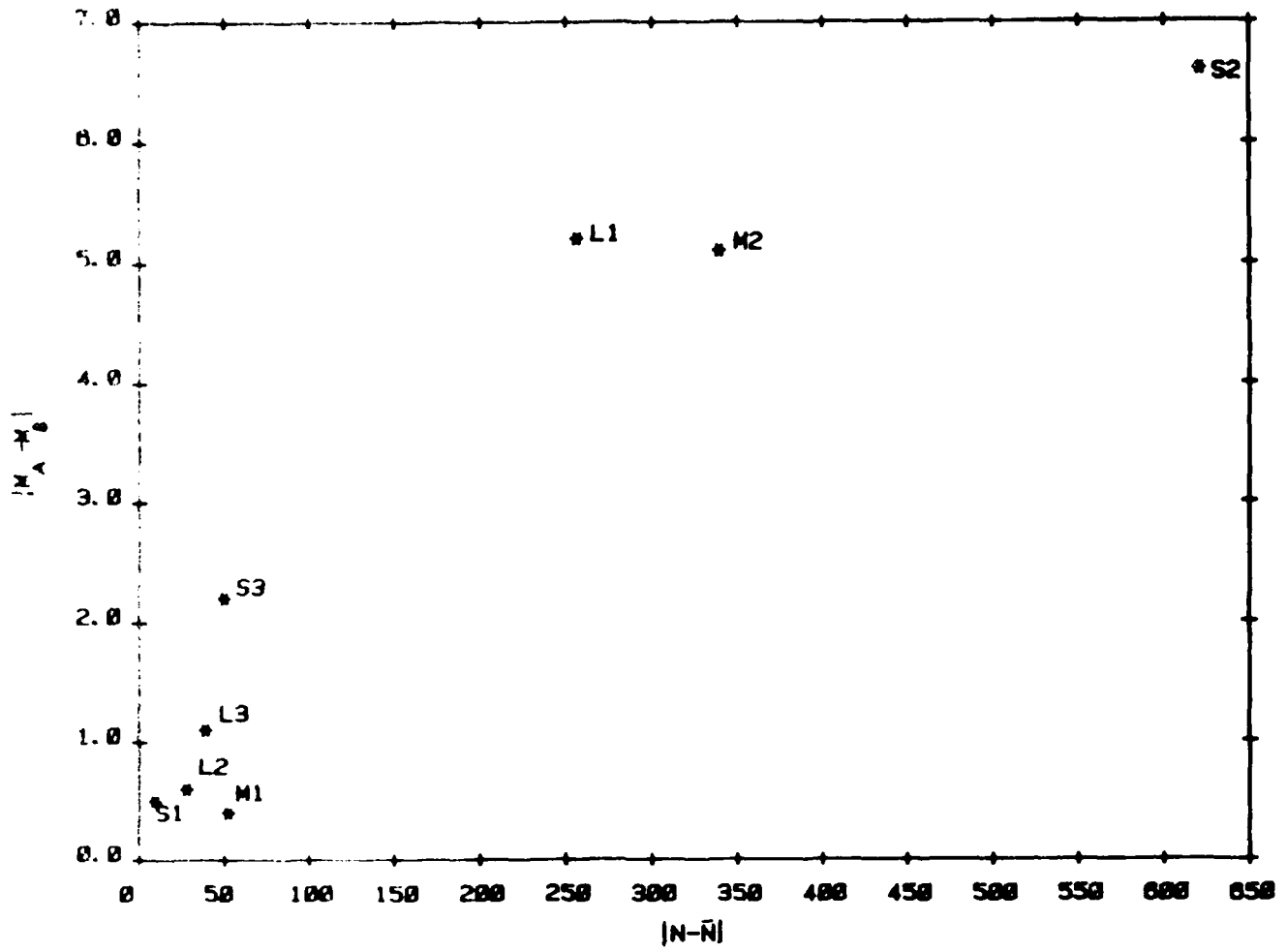

Figure 10. Graphic display of $|M_A-M_B|$ and $|N-\bar{N}|$ The specimens with FCG lives much different from the average had $|M_A-M_B|$ values exceeding 5.0 (L1, M2, S2). The other specimens, with lives nearest the average FCG life, had $|M_A-M_B|$ values of less than 2.3.

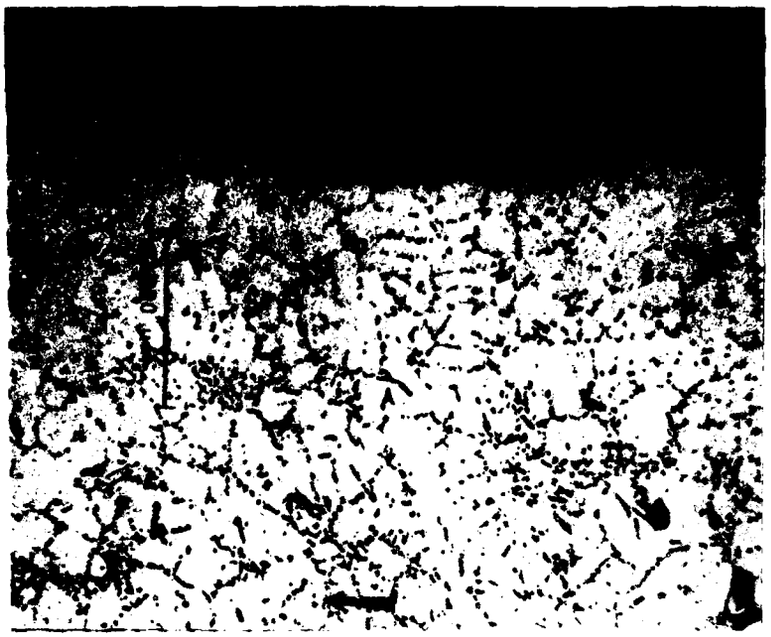

(a)

(b)

Figure 11. Crack path morphology at two different delta K levels in specimen L2: (a) 7 ksi-in$^{\frac{1}{2}}$, transdendritic, (b) 18 ksi-in$^{\frac{1}{2}}$, interdendritic. Arrows indicate crack propagation direction, Keller's etch, 100x.

Figure 12. Typical shrinkage porosity encountered by crack path. Specimen L2. Arrow indicates crack propagation direction. Kellers etch, 200x.

(a)

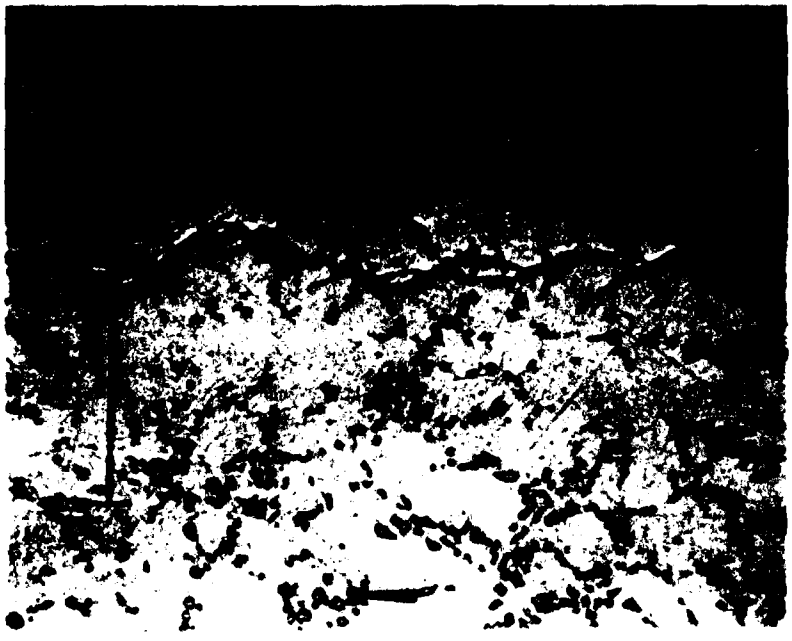

(b)

Figure 13. Examples of crack branching. (a) Specimen L2 (125x) (b) Specimen S2 (200x). Arrow indicates crack propagation direction, Keller's etch.

Plastic zone sizes were calculated with the hope of correlating the plastic zone size to a microstructural feature. This was done to determine if a microstructural feature was responsible for the reversals of FCGR at delta K of approximately 7.6 ksi in and the transition point from Stage II to Stage III of the FCGR plot. The cyclic plastic zone size was calculated using $r_y = (1/2\ )x(\text{delta K}/2x\ \text{yield strength})^2$. The plastic zone sizes at the reversal and the transition points were 0.0012 and 0.0032 inches, respectively. The plastic zone size of the reversal point (0.0012 in) was about the same as the average dendrite arm spacing (0.0014 in).

E. Fractographic Results

On a macroscopic level, the CT fracture faces were characterized by two regions. At low magnifications, the first region was coarsely faceted, while the second region was ductile and very irregular (Figure 14). Between the two regions, a short transition zone existed. For the most part, the fracture surfaces were very irregular, and by no means flat.

Since the fracture surfaces were so rough, it was decided that scanning electron microscopy would be more amenable for analyzing the surfaces than trying to produce replicas for transmission electron microscopy. Intensive SEM analyses were performed on specimens S2, M2 and L2, while cursory analyses were performed on the remaining specimens.

The first region appeared very ductile as evidenced by the dimpling of the surface (Figure 15). This was expected due to the transdendritic nature of the fracture revealed by the metallographic analysis. Occasionally, fatigue striations were found on the surface, but they were found locally (Figure 16).[20]

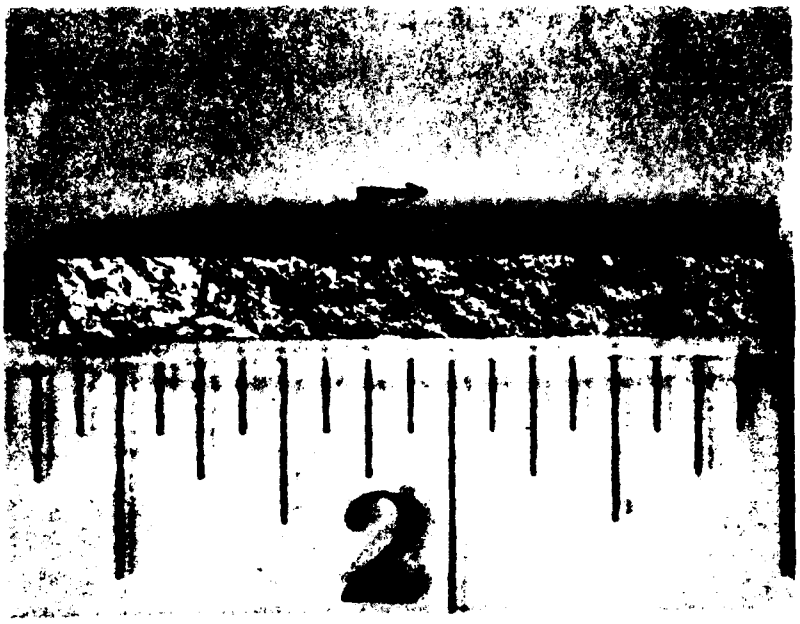

Figure 14. Typical macroscopic view of a fracture face. Note faceted appearance of region 1, and the transition of region 1 to region 2, and the ductile appearance of region 2. Arrow indicates crack propagation direction. Approximately 3x.

Figure 15. Region 1 fracture features. Note ductility, limited signs of fatigue, and lack of fractured silicon particles. 200x.

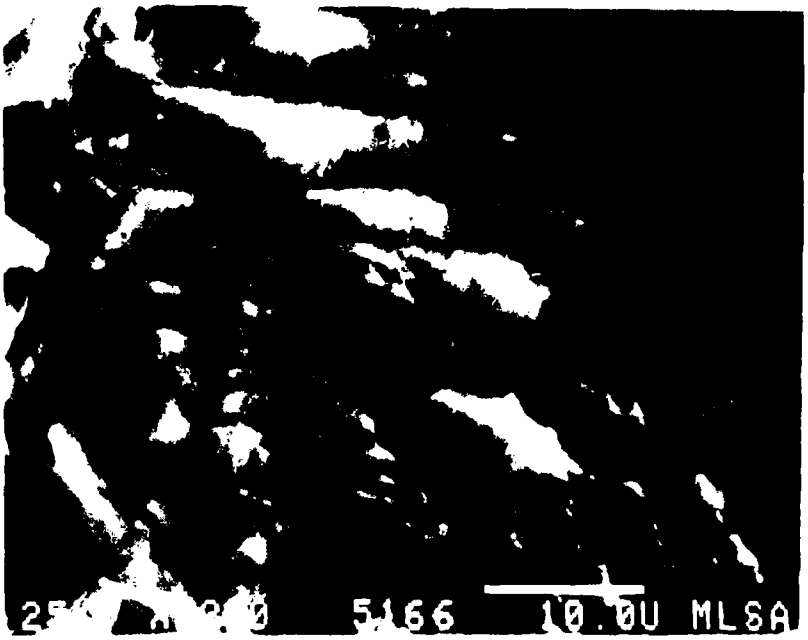

Figure 16. Localized region of fatigue striations on aluminum matrix. Also, fractured and secondary cracked silicon particle. 2200x

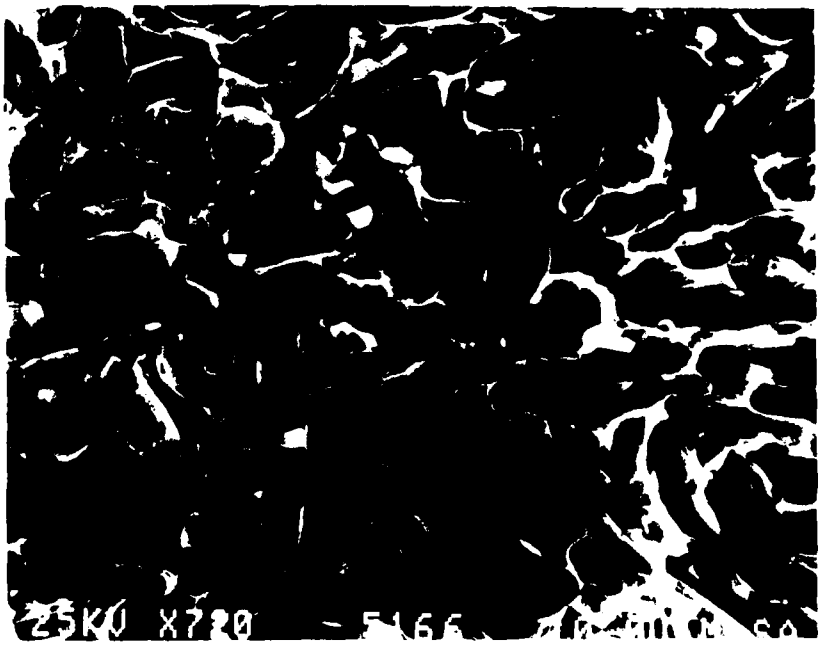

Figure 17. Region 2 fracture face characterized by fractured silicon particles indicating interdendritic nature of fracture.

The transition between the two regions was mixed with characteristics of Region 1 and Region 2, with no definitive transition point. Region 2, as shown in Figure 17, consisted of fractured and subcracked silicon particles in a ductile matrix. This, too, was expected. Earlier work on fracture toughness specimens showed the same effect as the Region 2 fracture morphology.[18]

Other features observed included porosity, subcracking, and crack branching. Figure 18 typifies the porosity scattered throughout the crack specimen.

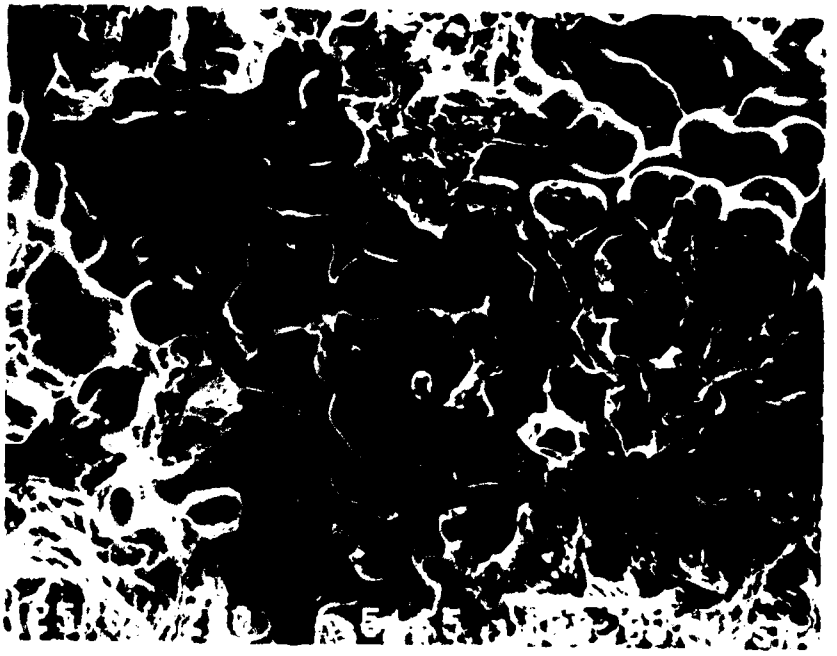

Figure 18. Shrinkage porosity typical of that scattered throughout the material. 200x

SECTION V
CONCLUSIONS

The variability of FCG life for premium quality casting alloy A357-T6 is higher than the variability of FCG life for a typical aerospace wrought alloy 2024-T3 as measured by the coefficient of variation of crack growth lives.

No conclusions can be drawn from this study concerning the correlation of measured microstructural features and FCG life and FCGR rates of A357-T6.

SECTION VI
RECOMMENDATIONS

It is believed that the eutectic silicon particles play a major role in both the fatigue and fracture of aluminum-silicon-magnesium casting alloys. Silicon particle parameters of size, shape, distribution and spacing, either together or independently, probably affect the fatigue and fracture properties the most as compared with the other microstructural features. A carefully controlled test program could be devised to evaluate damage tolerant properties by varying these parameters.

Another program would involve evaluating the effects of casting microstructures and discontinuties on threshold crack growth rates. To date, threshold values have not been published for premium quality castings, nor have the effects of microstructure and discontinuities on threshold values. Of particular interest would be the effects of porosity on crack growth at lower delta K values. One question that remains unanswered is: Would porosity serve to blunt or accelerate crack growth?

In a related, but different effort, the evolving technology of thermal analysis of molten aluminum could be applied towards predicting the fatigue and fracture properties of castings. Thermal analysis basically involves generating a cooling curve of the molten metal before the casting is poured. This cooling curve shows the amount of grain and silicon particle refinement the metal is capable of achieving. Although this technology is just evolving, and only tensile properties are predicted, it is believed that thermal analysis techniques can be applied to molten metal poured into fracture critical structures.

APPENDIX

What follows is a compilation of the raw FCG data acquired electronically and the FCGR data calculated using the 7-point polynomial method. This legend explains the abbreviations used.

Pmax is the maximum load applied in pounds force.

Pmin is the minimum load applied in pounds force.

R is the ratio of Pmin/Pmax=0.200.

B is the specimen thickness (See Figure 2a).

W is the specimen width (See Figure 2a).

Crack correction is the correction in factor used for the CT specimen.

Pt # is the sequential numbering system.

CYCLE COUNT is the number of cycles in thousands.

A-cor is the actual crack length read by the data acquisition system (Crack correction=0.000 inch).

A-reg is the crack length resulting from the seven point polynomial fit analysis.

MC is a measure of closeness of fit between A-cor and A-reg

delta K is the the calculated range of K values at [illegible] observation (units = ksi $\sqrt{in}$). If perfect fit MC = 1.0.

da/dN is the calculated crack growth rate at that delta K (units micro - in/cycle).

8 May 1985

SPECIMEN NO. S1

Pmax = 225 LBF Pmin = 45 LBF R = 0.200

B=0.122 in. W=2.000 in. Crack Correction =0.000 in.

PT #	CYCLE COUNT	A-cor in	A-seq in	MC	deltaK KSI$\sqrt{in}$	da/dn $\sqrt{in}$/cy
1	0.001	0.672				
2	52.770	0.688				
3	107.940	0.703				
4	167.600	0.718	0.717	0.999188	6.82	0.2421
5	239.320	0.734	0.733	0.997408	6.97	0.2283
6	319.770	0.749	0.750	0.997638	7.10	0.2333
7	390.740	0.765	0.766	0.997082	7.25	0.2676
8	442.400	0.780	0.780	0.994876	7.40	0.3284
9	495.940	0.795	0.798	0.995413	7.54	0.4223
10	530.900	0.811	0.813	0.994686	7.71	0.4630
11	553.160	0.826	0.824	0.990631	7.86	0.4616
12	579.830	0.841	0.839	0.998106	8.02	0.4921
13	617.090	0.857	0.857	0.998782	8.20	0.4564
14	654.030	0.872	0.872	0.999112	8.37	0.4069
15	692.330	0.887	0.886	0.996813	8.54	0.3948
16	740.430	0.903	0.904	0.994311	8.74	0.4383
17	779.260	0.918	0.921	0.996993	8.93	0.5155
18	803.770	0.933	0.933	0.998358	9.12	0.5653
19	827.010	0.949	0.947	0.997959	9.33	0.6072
20	851.510	0.964	0.964	0.999581	9.54	0.6565
21	875.090	0.979	0.979	0.995283	9.76	0.7252
22	899.090	0.995	0.996	0.996754	10.00	0.8415
23	918.350	1.010	1.013	0.994488	10.23	1.0626
24	929.540	1.026	1.024	0.985615	10.49	1.3717
25	944.610	1.041	1.047	0.985954	10.75	1.9799
26	950.840	1.056	1.059	0.990699	11.01	2.4702
27	954.940	1.072	1.068	0.996045	11.31	2.8905
28	960.830	1.087	1.088	0.992015	11.60	3.6440
29	965.500	1.102	1.105	0.986003	11.90	4.8353
30	968.870	1.118	1.121	0.995410	12.23	6.2586
31	970.800	1.133	1.133	0.996829	12.56	7.0638
32	972.320	1.148	1.145	0.994910	12.91	8.1133
33	974.640	1.164	1.166	0.976814	13.30	10.6716
34	976.420	1.179	1.186	0.971892	13.68	16.2019
35	977.280	1.194	1.201	0.968099	14.08	24.8703
36	977.650	1.210	1.209	0.989062	14.53	34.4554
37	978.240	1.225	1.231	0.986384	14.97	49.5391
38	978.360	1.240	1.236	0.985514	15.44	56.6989
39	978.750	1.256	1.260	0.988463	15.97	81.2064
40	978.870	1.271	1.269	0.985674	16.49	100.7436
41	979.060	1.287	1.289	0.996057	17.08	128.8119
42	979.160	1.302	1.303	0.995693	17.67	140.6520
43	979.240	1.318	1.314	0.989681	18.33	165.0695
44	979.350	1.333	1.334	0.957895	18.99	240.1842
45	979.450	1.349				
46	979.480	1.366				
47	979.520	1.395				

*-data violates specimen size requirements

Paris exponent 7.218

log of intercept -12.979

Paris coefficient $1.049*10^{-}$ -13.000

A357-T6, S1

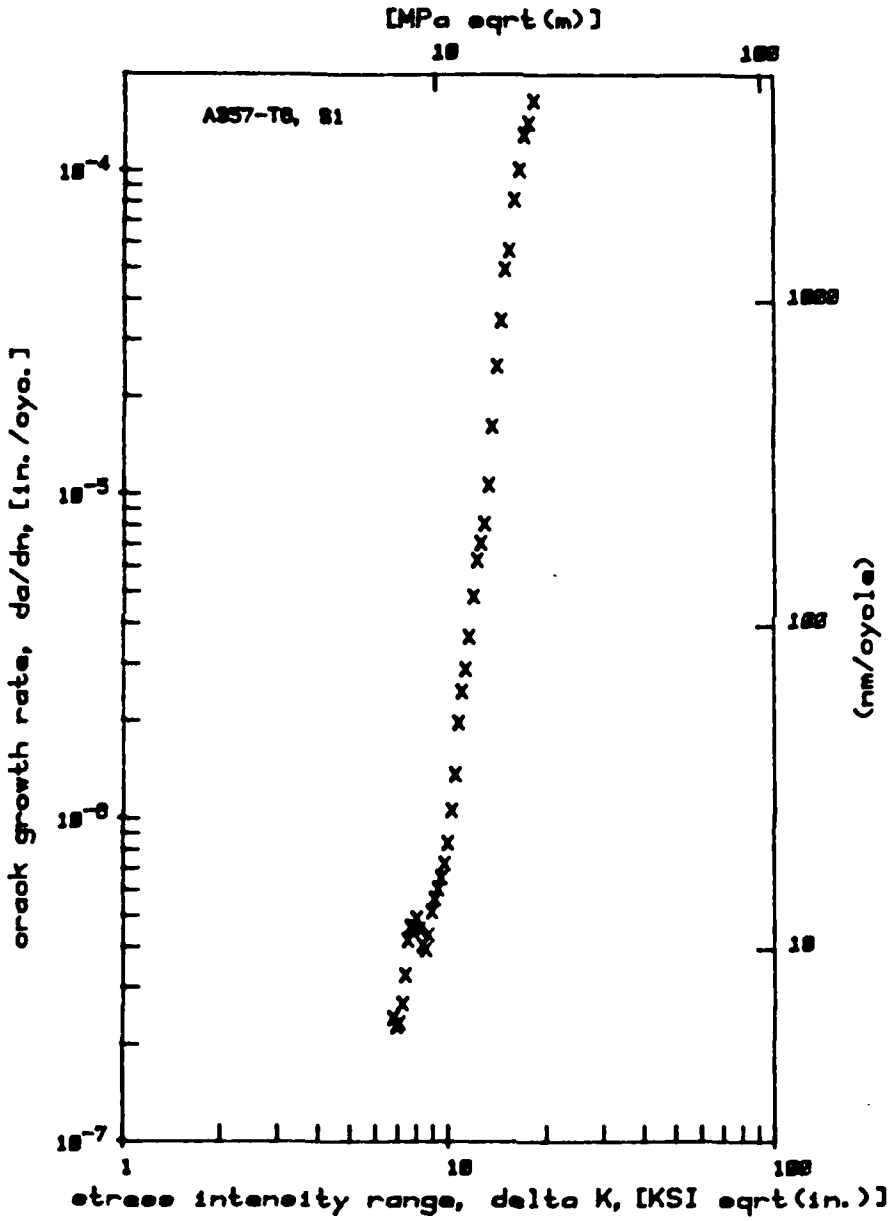
[MPa sqrt(m)]
10
100
A357-T6, S1
10^{-4}
10^{-5}
10^{-6}
10^{-7}
1000
100
10
crack growth rate, da/dn, [in./cyc.]
(nm/cycle)
1
10
100
stress intensity range, delta K, [KSI sqrt(in.)]

8 May 1985

SPECIMEN NO. S2

Pmax = 225 LBF Pmin = 45 LBF R = 0.200

B=0.122 in. W=1.999 in. Crack Correction =0.000 in.

PT #	CYCLE COUNT	A-cor in	A-sec in	MC	delta KSI√in	da/dn in/cy
1	0.001	0.683				
2	106.590	0.698				
3	218.890	0.713				
4	330.920	0.729	0.731	0.999197	6.93	0.1629
5	403.050	0.744	0.742	0.999307	7.06	0.1720
6	496.050	0.759	0.759	0.998700	7.20	0.1905
7	580.570	0.775	0.775	0.995839	7.35	0.2214
8	653.880	0.790	0.791	0.996847	7.50	0.2720
9	709.520	0.805	0.807	0.996991	7.65	0.3037
10	751.990	0.821	0.821	0.994773	7.81	0.3143
11	787.280	0.836	0.834	0.997368	7.97	0.3261
12	839.640	0.851	0.851	0.998752	8.14	0.3237
13	891.450	0.867	0.867	0.998804	8.32	0.3065
14	945.420	0.882	0.882	0.999288	8.49	0.3074
15	996.600	0.898	0.898	0.999334	8.68	0.3240
16	1046.550	0.913	0.914	0.999018	8.87	0.3334
17	1083.740	0.928	0.927	0.997923	9.06	0.3579
18	1127.710	0.944	0.943	0.997028	9.28	0.3944
19	1175.390	0.959	0.962	0.996891	9.48	0.4273
20	1201.070	0.974	0.974	0.994716	9.70	0.4200
21	1232.140	0.990	0.988	0.995304	9.93	0.4380
22	1268.640	1.005	1.004	0.994245	10.17	0.4661
23	1310.550	1.020	1.023	0.996255	10.41	0.4967
24	1339.780	1.036	1.037	0.998818	10.67	0.5509
25	1362.510	1.051	1.049	0.998061	10.94	0.6316
26	1388.550	1.066	1.067	0.998060	11.21	0.7085
27	1411.560	1.082	1.084	0.995006	11.51	0.8407
28	1425.040	1.097	1.095	0.996247	11.81	0.9303
29	1445.860	1.112	1.116	0.994005	12.12	1.0025
30	1454.840	1.128	1.126	0.994432	12.47	1.0142
31	1469.130	1.143	1.140	0.993850	12.81	1.0284
32	1487.230	1.159	1.160	0.993064	13.19	1.0868
33	1503.440	1.174	1.176	0.998489	13.57	1.1334
34	1514.530	1.189	1.188	0.999051	13.96	1.2437
35	1526.430	1.205	1.204	0.998816	14.41	1.4027
36	1538.670	1.220	1.222	0.996127	14.84	1.6738
37	1546.910	1.235	1.235	0.997273	15.31	1.9740
38	1555.600	1.251	1.253	0.999193	15.83	2.3604
39	1560.590	1.266	1.265	0.999153	16.34	2.5873
40	1566.070	1.281	1.280	0.998584	16.88	2.9318
41	1571.740	1.297	1.299	0.994713	17.50	2.9099
42	1576.460	1.312	1.313	0.994975	18.11	2.8218
43	1579.800	1.327	1.322	0.989188	18.75	2.9007
44	1588.110	1.343				
45	1594.130	1.358				
46	1596.470	1.373				

*-data violates specimen size requirements

Paris exponent 2.927

log of intercept -9.210

Paris coefficient 6.161*10^ -10.000

A357-T6, S2

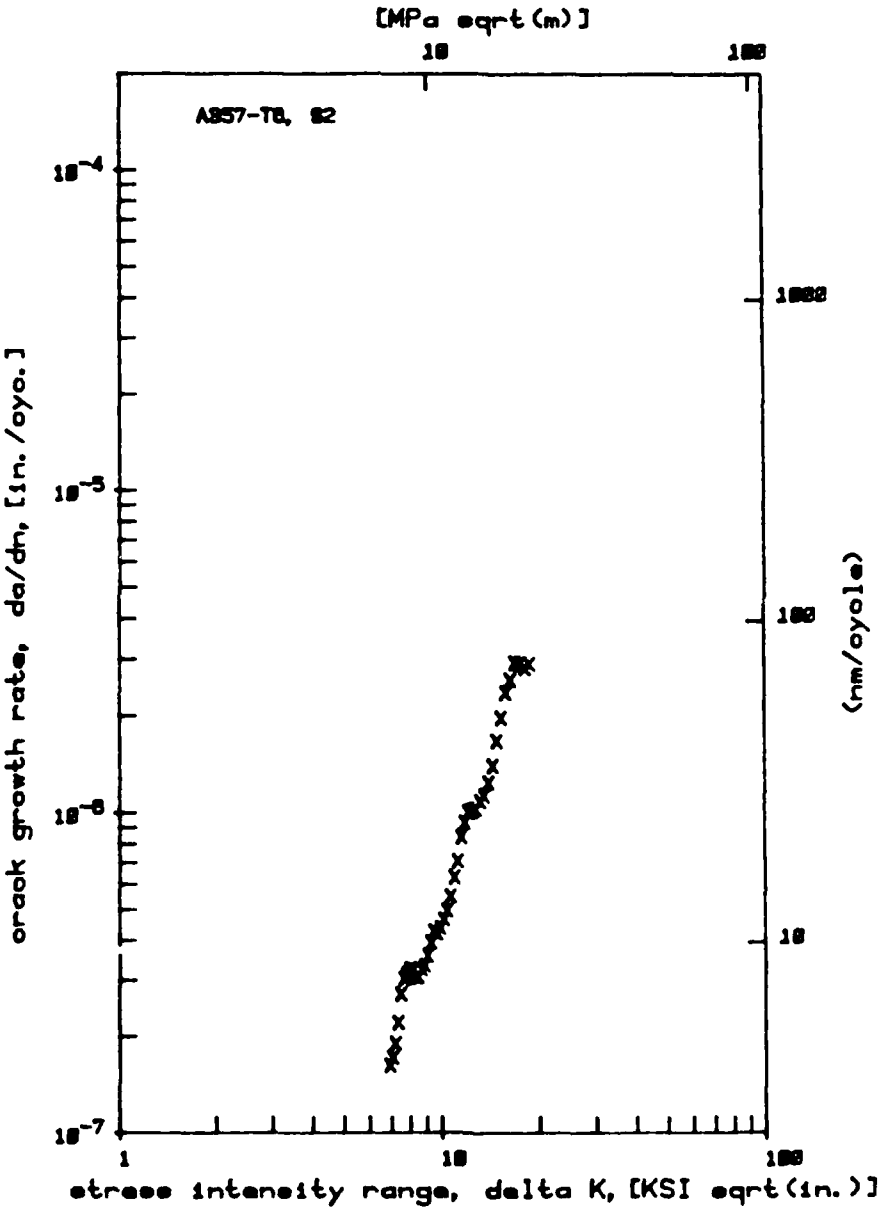
[MPa sqrt(m)]
10
100
A357-T6, S2
10^{-4}
10^{-5}
10^{-6}
10^{-7}
1000
100
10
crack growth rate, da/dn, [in./cycle]
(nm/cycle)
1
10
100
stress intensity range, delta K, [KSI sqrt(in.)]

8 May 1985

SPECIMEN NO. 63

Pmax = 225 LBF Pmin = 45 LBF P = 0.200

B=0.121 in. W=2.000 in. Crack Correction =0.000 in.

PT #	CYCLE COUNT	A-cor in	A-meg in	MC	deltaK KSI√in	da/dn min/cy
1	0.001	0.657				
2	69.390	0.672				
3	132.710	0.688				
4	189.360	0.703	0.702	0.999687	6.75	0.2563 *
5	253.020	0.718	0.720	0.998313	6.88	0.2540
6	309.900	0.734	0.734	0.998496	7.02	0.2480
7	360.840	0.749	0.747	0.998488	7.16	0.2423
8	438.890	0.764	0.765	0.995565	7.30	0.2413
9	509.860	0.780	0.780	0.992210	7.46	0.2696
10	574.880	0.795	0.798	0.993932	7.61	0.3468
11	616.710	0.810	0.812	0.997391	7.76	0.4265
12	648.160	0.826	0.825	0.999031	7.93	0.4896
13	674.660	0.841	0.840	0.999444	8.09	0.5460
14	703.180	0.856	0.857	0.998103	8.25	0.5604
15	729.630	0.872	0.873	0.997947	8.44	0.5486
16	750.960	0.887	0.885	0.998441	8.61	0.5315
17	784.740	0.902	0.902	0.996395	8.80	0.5018
18	820.290	0.918	0.917	0.992612	9.00	0.4960
19	858.890	0.933	0.935	0.991263	9.19	0.6001
20	885.580	0.949	0.951	0.993480	9.41	0.7869
21	903.590	0.964	0.965	0.999237	9.62	0.9614
22	916.190	0.979	0.978	0.998960	9.84	1.1204
23	930.060	0.995	0.994	0.998659	10.08	1.3116
24	942.860	1.010	1.012	0.998551	10.32	1.5211
25	950.960	1.025	1.024	0.997839	10.56	1.7661
26	960.290	1.041	1.041	0.998536	10.84	2.0718
27	967.920	1.056	1.058	0.998178	11.10	2.2790
28	972.580	1.071	1.069	0.998194	11.38	2.4457
29	979.270	1.087	1.086	0.996451	11.69	2.8160
30	985.490	1.102	1.104	0.990343	12.00	3.4975
31	989.860	1.117	1.119	0.990276	12.31	4.6646
32	993.440	1.133	1.137	0.981778	12.67	6.9356
33	995.390	1.148	1.152	0.969544	13.02	10.4198
34	997.230	1.164	1.175	0.958341	13.41	17.9221
35	997.720	1.179	1.183	0.962454	13.79	29.4841
36	998.190	1.194	1.197	0.990912	14.20	47.7170
37	998.520	1.210	1.213	0.995777	14.65	60.6414
38	998.710	1.225	1.224	0.994918	15.10	73.7271
39	998.880	1.240	1.238	0.983036	15.57	92.8410
40	999.130	1.256	1.264	0.965829	16.10	146.1030
41	999.210	1.271	1.276	0.972921	16.63	223.3797
42	999.270	1.287				
43	999.310	1.302				
44	999.350	1.317				

*-data violates specimen size requirements

Paris exponent 7.377

log of intercept -13.091

Paris coefficient 8.105*10^ -14.000

A357-T6, S3

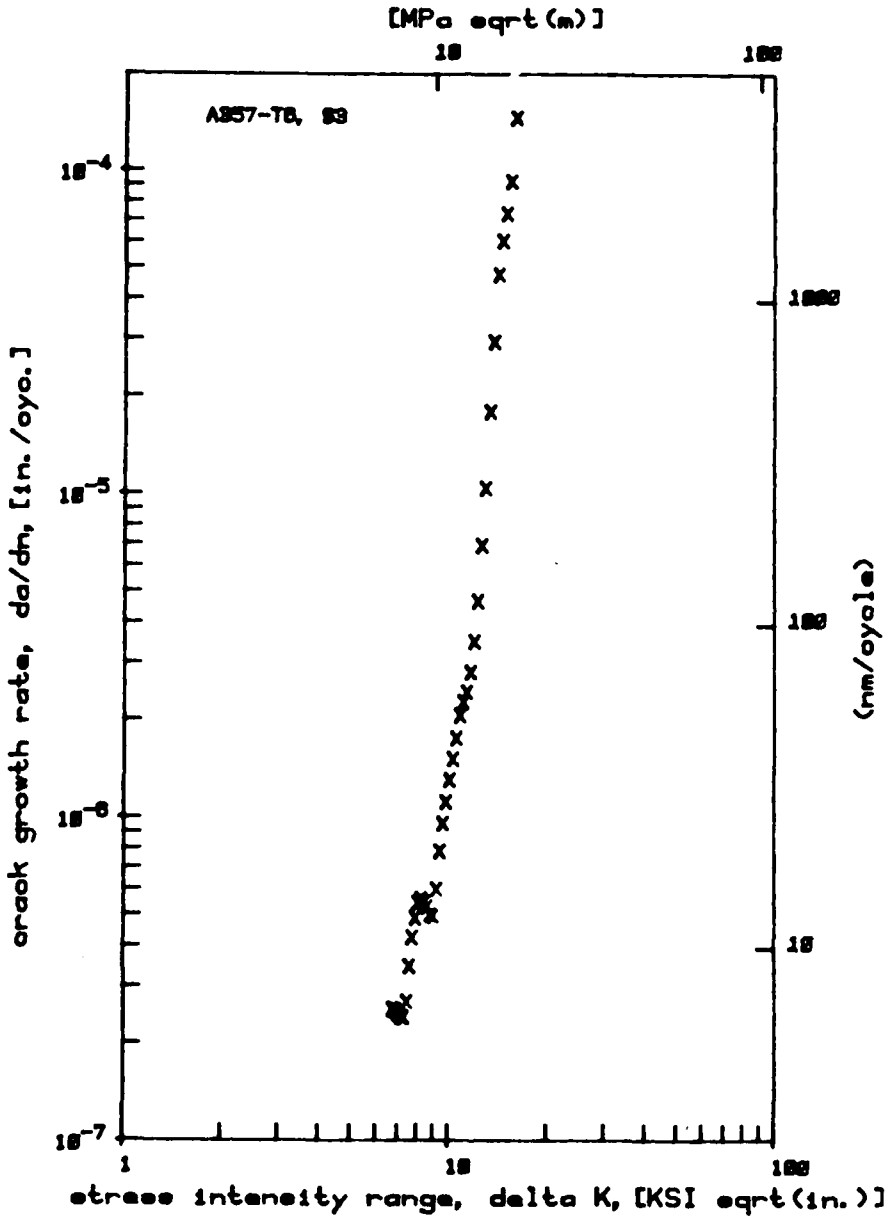
[MPa sqrt(m)]
10
100
A357-T6, S3
10^{-4}
10^{-5}
10^{-6}
10^{-7}
1000
100
10
crack growth rate, da/dn, [in./cyc.]
(nm/cycle)
1
10
100
stress intensity range, delta K, [KSI sqrt(in.)]

8 May 1985

SPECIMEN NO. M1

Pmax = 225 LBF Pmin = 45 LBF R = 0.200

B=0.121 in. W=2.000 in Crack Correction =0.000 in.

PT #	CYCLE COUNT	A-cor in	A-avg in	MC	delta K KSI√in	da/dn in/cy
1	0.001	0.671				
2	57.820	0.687				
3	112.180	0.702				
4	175.360	0.717	0.717	0.999748	6.87	0.2409
5	240.400	0.733	0.732	0.999660	7.02	0.2259
6	317.430	0.748	0.748	0.999570	7.15	0.2130
7	387.580	0.763	0.763	0.999351	7.29	0.2087
8	470.340	0.779	0.779	0.997995	7.45	0.2196
9	541.890	0.794	0.794	0.994291	7.60	0.2569
10	608.410	0.809	0.811	0.995583	7.75	0.3223
11	655.280	0.825	0.827	0.998093	7.92	0.4041
12	685.770	0.840	0.839	0.998979	8.08	0.4850
13	718.910	0.855	0.856	0.998883	8.24	0.5825
14	745.710	0.871	0.872	0.998885	8.43	0.6864
15	764.560	0.886	0.885	0.999567	8.60	0.7895
16	785.600	0.902	0.903	0.999088	8.80	0.9401
17	801.180	0.917	0.918	0.998447	8.99	1.1090
18	814.310	0.932	0.932	0.999606	9.18	1.2601
19	826.450	0.948	0.949	0.993959	9.40	1.2576
20	835.270	0.963	0.962	0.996347	9.61	1.3027
21	845.700	0.978	0.975	0.995234	9.83	1.3335
22	862.510	0.994	0.996	0.991280	10.07	1.4422
23	872.700	1.009	1.010	0.992667	10.30	1.7731
24	881.500	1.024	1.026	0.997888	10.55	2.1132
25	888.300	1.040	1.041	0.997939	10.82	2.4226
26	892.700	1.055	1.052	0.997693	11.09	2.5707
27	899.590	1.070	1.071	0.994855	11.36	2.9828
28	904.470	1.086	1.085	0.993497	11.67	3.4555
29	909.870	1.101	1.105	0.996029	11.97	3.9519
30	912.300	1.116	1.114	0.993106	12.29	4.5034
31	915.600	1.132	1.130	0.987859	12.64	5.5187
32	919.550	1.147	1.154	0.968923	12.99	8.2357
33	921.040	1.163	1.168	0.950028	13.38	12.8307
34	922.400	1.178	1.186	0.976202	13.77	18.3788
35	922.830	1.193	1.194	0.968658	14.17	17.3192
36	923.110	1.209	1.200	0.968514	14.62	19.3379
37	924.310	1.224	1.226	0.943872	15.07	22.7784
38	925.350	1.239	1.250	0.928974	15.54	39.3231
39	925.650	1.255	1.267	0.903834	16.07	62.6396
40	925.750	1.270	1.280	0.768914	16.59	179.4446
41	925.900	1.285				
42	925.940	1.301				
43	925.970	1.368				

*-data violates specimen size requirements

Paris exponent 6.609

log of intercept -12.356

Paris coefficient 4.408*10^ -13.000

A357-T6, M1

Copy ... not permit fully legible reproduction

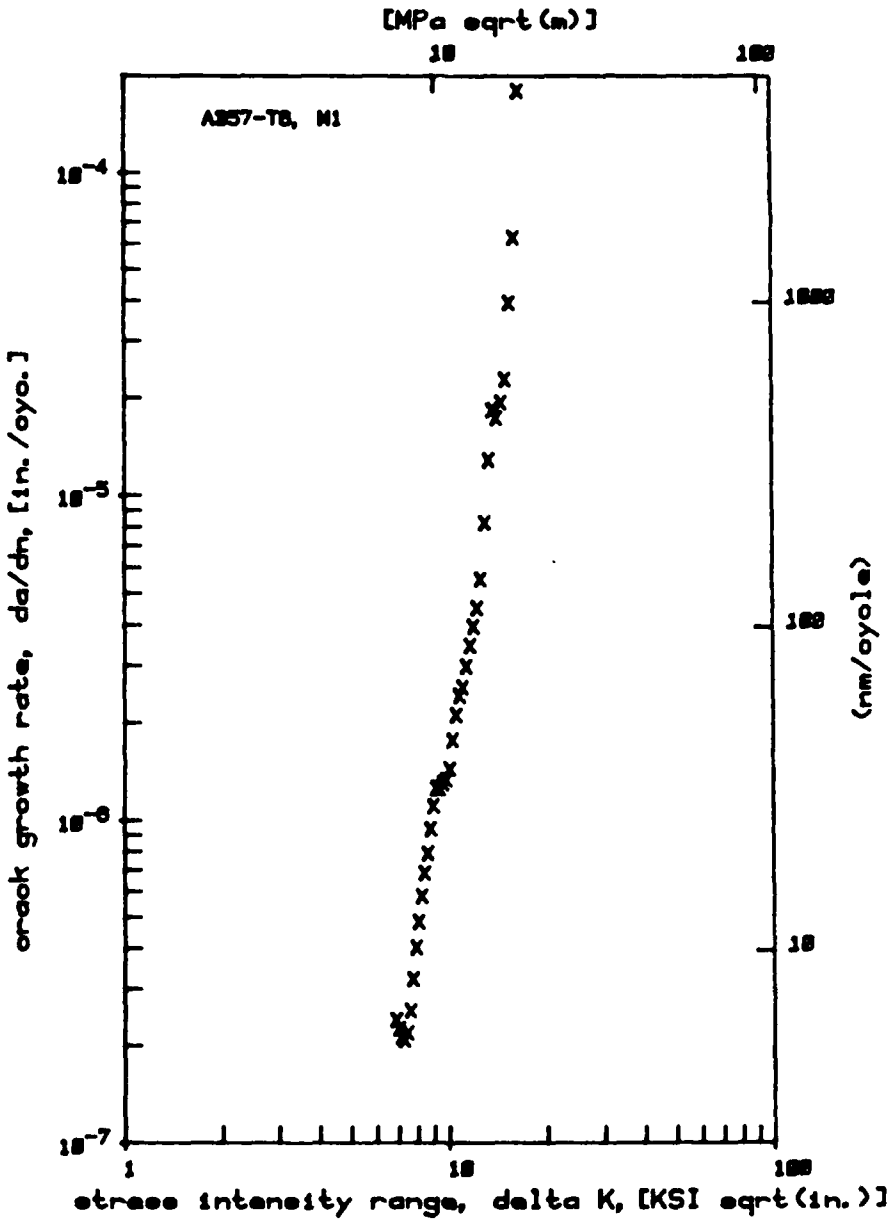
[MPa sqrt(m)]
10
100
A357-T6, N1
10^{-4}
10^{-5}
10^{-6}
10^{-7}
1000
100
10
crack growth rate, da/dn, [in./cyc.]
(nm/cycle)
1
10
100
stress intensity range, delta K, [KSI sqrt(in.)]

SPECIMEN NO. M2

Pmax = 225 LBF Pmin = 45 LBF R = 0.200

B=0.122 in. W=2.000 in Crack Correction =0.000 in

PT #	CYCLE COUNT	A-ccr in	A-ieq in	MC	delta K ksi√in	da/dn ulmacy
1	0.001	0.673				
2	41.900	0.688				
3	86.920	0.704				
4	128.710	0.719	0.720	0.998934	6.83	0.4238
5	164.600	0.734	0.736	0.998187	6.97	0.4422
6	193.110	0.750	0.749	0.997544	7.11	0.4510
7	223.530	0.765	0.764	0.998870	7.25	0.4667
8	261.630	0.781	0.781	0.998705	7.41	0.4680
9	296.550	0.796	0.797	0.999452	7.55	0.4595
10	326.090	0.811	0.810	0.999477	7.71	0.4695
11	358.880	0.827	0.826	0.998619	7.87	0.5015
12	393.570	0.842	0.843	0.996696	8.03	0.5688
13	419.920	0.857	0.858	0.998343	8.20	0.6297
14	443.760	0.873	0.873	0.998311	8.38	0.7347
15	460.470	0.888	0.886	0.996096	8.56	0.8537
16	482.910	0.903	0.906	0.996182	8.74	1.0431
17	495.960	0.919	0.920	0.996998	8.94	1.1584
18	506.310	0.934	0.932	0.996506	9.13	1.2266
19	517.910	0.949	0.949	0.999145	9.33	1.2827
20	530.310	0.965	0.965	0.996292	9.56	1.3059
21	541.440	0.980	0.978	0.992916	9.77	1.3884
22	557.290	0.996	1.001	0.990450	10.02	1.7700
23	563.710	1.011	1.011	0.994632	10.25	1.9830
24	570.740	1.026	1.026	0.993107	10.49	2.4430
25	576.190	1.042	1.040	0.992675	10.77	2.8285
26	583.620	1.057	1.062	0.993268	11.03	3.2329
27	585.740	1.072	1.070	0.990924	11.31	3.1799
28	590.430	1.088	1.085	0.984295	11.62	3.5653
29	595.140	1.103	1.104	0.985849	11.92	3.8531
30	600.430	1.118	1.124	0.989408	12.23	3.7959
31	601.710	1.134	1.128	0.988267	12.59	3.9579
32	606.400	1.149	1.147	0.979289	12.93	4.6317
33	610.930	1.164	1.169	0.962685	13.30	6.6847
34	613.330	1.180	1.186	0.982357	13.70	9.0699
35	614.550	1.195	1.196	0.992253	14.11	11.5280
36	615.260	1.210	1.204	0.987189	14.53	13.3778
37	617.050	1.226	1.231	0.980454	15.00	18.8020
38	617.750	1.241	1.243	0.988608	15.47	23.5222
39	618.270	1.257	1.255	0.997052	16.00	27.2014
40	618.740	1.272	1.270	0.989437	16.53	33.0999
41	619.310	1.287	1.290	0.971692	17.08	44.9484
42	619.770	1.304	1.313	0.978296	17.75	67.4147
43	619.880	1.319	1.319	0.978513	18.37	89.7755
44	620.000	1.334	1.330	0.957611	19.02	121.9091
45	620.230	1.350				
46	620.260	1.366				
47	620.290	1.383				

*-data violates specimen size requirements

Paris exponent 5.395

log of intercept -11.097

Paris coefficient 8.004*10^ -12.000

A357-T6, M2

Copy available to DTIC does not permit fully legible reproduction

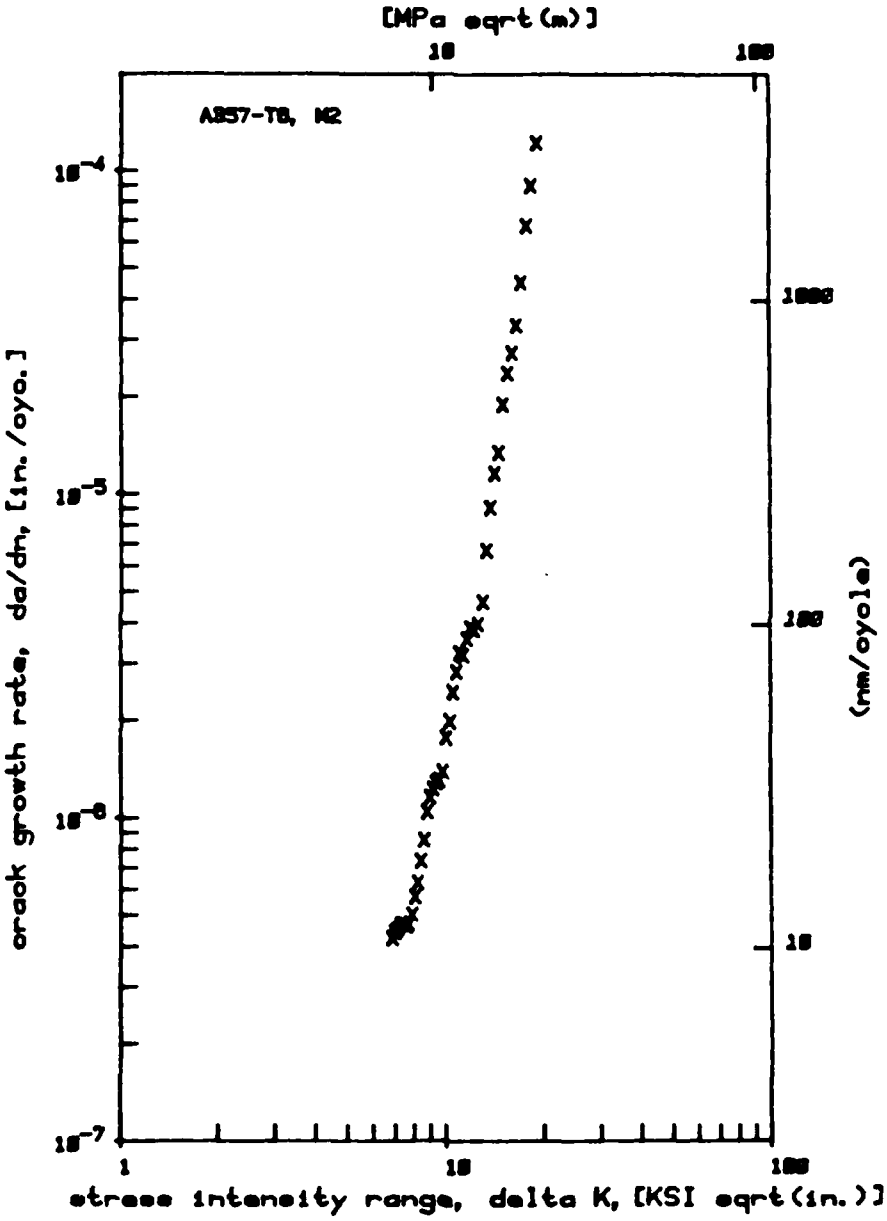
[MPa sqrt(m)]
10
100
A357-T6, N2
10^{-4}
10^{-5}
10^{-6}
10^{-7}
1000
100
10
(nm/cycle)
crack growth rate, da/dn, [in./cyc.]
1
10
100
stress intensity range, delta K, [KSI sqrt(in.)]

8 May 1985

SPECIMEN NO. M3

Pmax = 300 LBF Pmin = 60 LBF P = 0.200

B=0.122 in. W=2.001 in. Crack Correction =0.000 in.

PT #	CYCLE COUNT	A-cor in	A-seq in	MC	delta KSI√in	da/dn uin/cy
1	0.001	0.690				
2	294.450	0.705				
3	444.150	0.721				
4	626.110	0.736	0.748	0.927560	9.31	0.1973
5	688.650	0.751	0.765	0.889601	9.49	0.3784
6	708.690	0.767	0.776	0.935677	9.69	0.7977
7	718.310	0.782	0.781	0.998182	9.88	1.3617
8	730.130	0.797	0.798	0.994353	10.08	1.7829
9	738.790	0.813	0.814	0.994897	10.29	2.1119
10	746.350	0.828	0.831	0.996343	10.50	2.5603
11	749.730	0.843	0.839	0.996263	10.72	2.7904
12	757.000	0.859	0.862	0.995486	10.95	3.1194
13	760.600	0.874	0.874	0.995945	11.18	3.2251
14	764.760	0.889	0.887	0.995758	11.41	3.1564
15	770.050	0.905	0.906	0.999050	11.67	3.2808
16	774.530	0.920	0.919	0.992159	11.92	3.3875
17	780.230	0.936	0.938	0.977839	12.20	4.3471
18	784.640	0.951	0.959	0.975234	12.47	6.6971
19	786.290	0.966	0.969	0.983789	12.75	9.5161
20	787.600	0.982	0.981	0.987146	13.06	13.8638
21	788.970	0.997	1.002	0.989072	13.36	18.1965
22	789.700	1.012	1.015	0.988357	13.67	19.7088
23	790.040	1.028	1.022	0.986870	14.02	19.9460
24	790.910	1.043	1.043	0.988705	14.36	23.1633
25	791.680	1.058	1.059	0.978124	14.72	27.0979
26	792.420	1.074	1.081	0.974460	15.11	40.9093
27	792.730	1.089	1.093	0.979754	15.50	60.8005
28	792.980	1.105	1.108	0.997495	15.93	85.3400
29	793.120	1.121	1.120	0.997574	16.38	104.7331
30	793.260	1.136	1.136	0.978381	16.82	139.6186
31	793.400	1.151	1.158	0.940184	17.29	262.6954
32	793.480	1.167	1.178	0.976847	17.81	373.4934
33	793.490	1.182				
34	793.570	1.226				
35	793.640	1.253				

*-data violates specimen size requirements

Paris exponent 9.569

log of intercept -15.579

Paris coefficient 2.636*10^ -16.000

A357-T6, M3

Copy available to DTIC does not permit fully legible reproduction

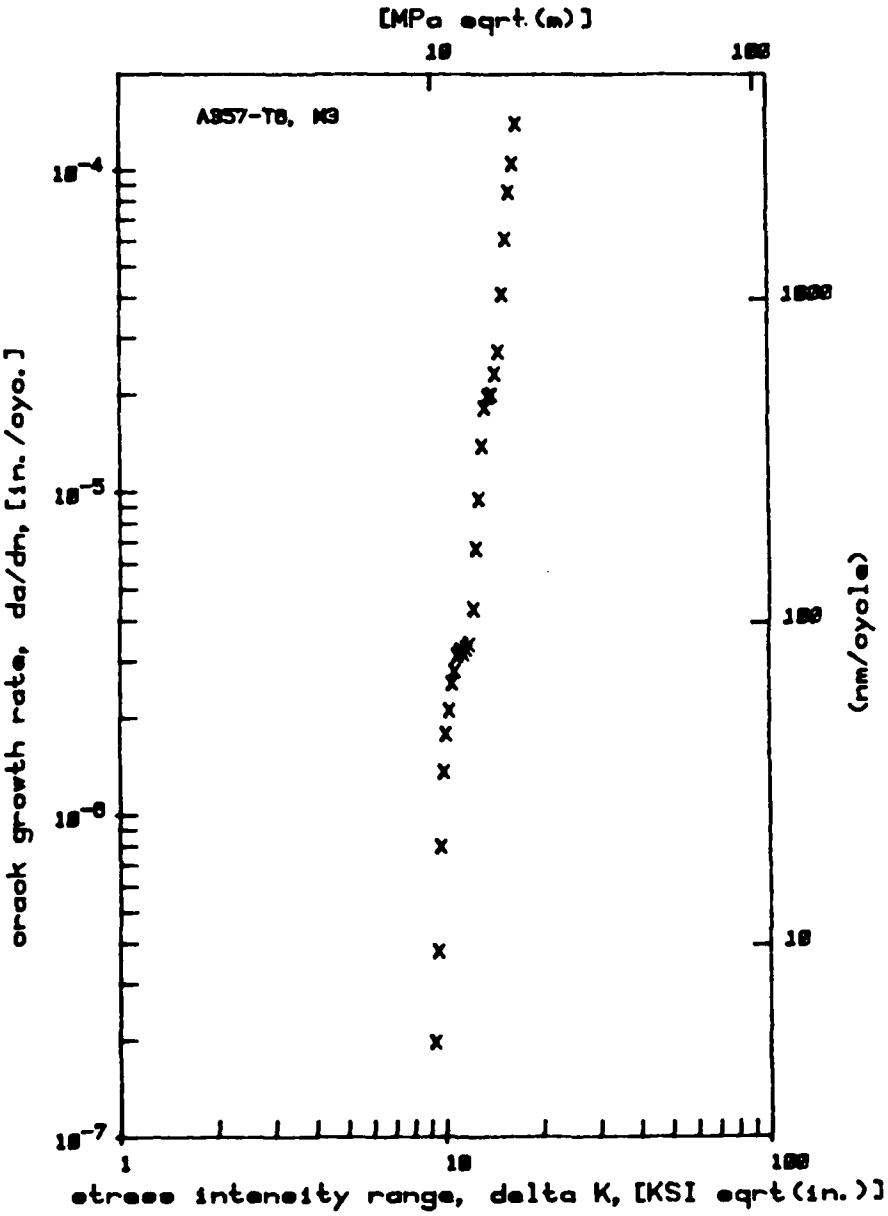
[MPa sqrt.(m)]
10
100
A357-T6, N3
10^{-4}
10^{-5}
10^{-6}
10^{-7}
1000
100
10
crack growth rate, da/dn, [in./cyc.]
(nm/cycle)
1
10
100
stress intensity range, delta K, [KSI sqrt(in.)]

8 May 1985

SPECIMEN NO. L1

Pmax = 225 LBF Pmin = 45 LBF P = 0.200

B=0.120 in. W=2.001 in. Crack Correction =0.000 in.

PT #	CYCLE COUNT	A-cor in	A-sieq in	MC	deltaK KSI√in	da/dn in/cy
1	0.001	0.677				
2	38.850	0.693				
3	98.740	0.708				
4	136.270	0.723	0.725	0.995818	6.96	0.3991
5	165.700	0.739	0.737	0.991642	7.12	0.3888
6	201.200	0.754	0.754	0.998750	7.26	0.4089
7	240.690	0.770	0.769	0.998040	7.42	0.3868
8	289.170	0.785	0.786	0.999143	7.56	0.3536
9	332.800	0.800	0.800	0.998989	7.71	0.3475
10	376.070	0.816	0.815	0.999272	7.88	0.3565
11	424.800	0.831	0.832	0.998610	8.04	0.3900
12	460.690	0.846	0.846	0.997837	8.20	0.4408
13	498.500	0.862	0.863	0.997769	8.38	0.5396
14	526.960	0.877	0.878	0.998382	8.56	0.6486
15	548.540	0.892	0.893	0.998560	8.74	0.7868
16	567.020	0.908	0.907	0.994556	8.94	0.9961
17	584.740	0.923	0.926	0.995935	9.13	1.2234
18	595.580	0.938	0.939	0.996865	9.33	1.4125
19	603.350	0.954	0.950	0.997127	9.55	1.5632
20	614.990	0.969	0.971	0.996685	9.77	1.6655
21	622.560	0.984	0.985	0.996832	9.99	1.6582
22	630.240	1.000	0.997	0.995845	10.23	1.6640
23	641.340	1.015	1.016	0.995324	10.48	1.7543
24	651.920	1.031	1.033	0.988616	10.74	2.0859
25	658.240	1.046	1.046	0.980995	11.00	2.7657
26	665.640	1.061	1.068	0.985381	11.28	3.9650
27	668.250	1.077	1.078	0.984053	11.58	4.1461
28	670.200	1.092	1.087	0.983797	11.88	4.5234
29	673.740	1.107	1.106	0.982243	12.19	5.4799
30	678.040	1.123	1.129	0.974810	12.53	7.5242
31	679.720	1.138	1.141	0.988802	12.87	9.8444
32	681.030	1.153	1.153	0.996071	13.23	11.5549
33	682.010	1.169	1.166	0.995415	13.63	13.3374
34	683.320	1.184	1.184	0.991690	14.02	16.0770
35	684.470	1.199	1.204	0.988699	14.43	16.6443
36	685.050	1.215	1.214	0.982551	14.90	18.7529
37	685.630	1.230	1.226	0.960401	15.36	22.5601
38	686.920	1.246	1.262	0.909905	15.87	37.7133
39	687.070	1.261	1.269	0.882316	16.38	76.0305
40	687.230	1.276	1.286	0.947439	16.92	171.3375
41	687.310	1.292				
42	687.360	1.308				
43	687.380	1.327				

*-data violates specimen size requirements

Paris exponent 6.287

log of intercept -11.997

Paris coefficient 1.008*10^ -12.000

A357-T6, L1

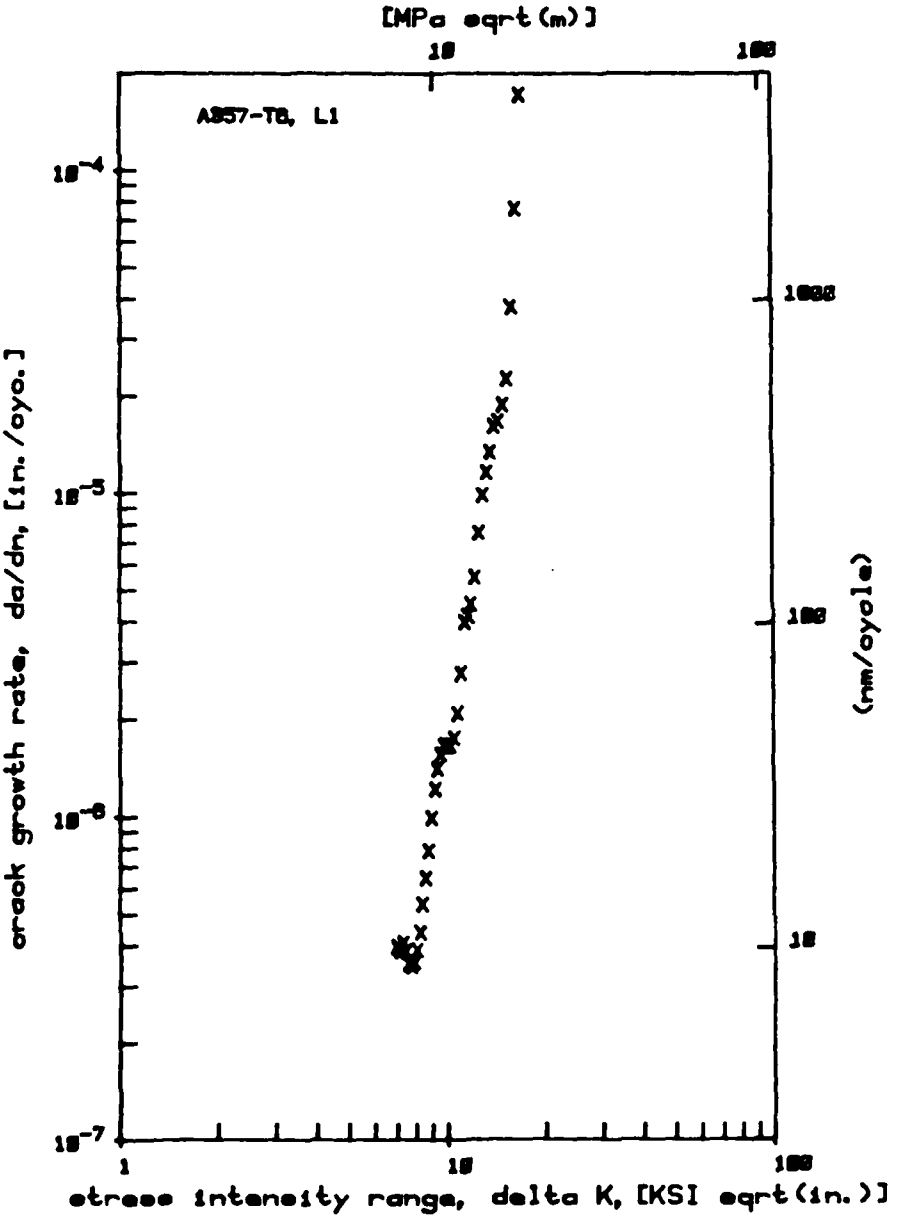
[MPa sqrt(m)]
10
100
A357-T6, L1
10^{-4}
10^{-5}
10^{-6}
10^{-7}
1000
100
10
crack growth rate, da/dn, [in./cyc.]
(mm/cycle)
1
10
100
stress intensity range, delta K, [KSI sqrt(in.)]

8 May 1985

SPECIMEN NO. L2

Pmax = 225 LBF Pmin = 45 LBF P = 0.200

B=0.121 in. W=2.000 in. Crack Correction =0.000 in.

PT #	CYCLE COUNT	A-cor in	A-meg in	MC	deltaK KSI√in	da/dn in/cy
1	0.001	0.671				
2	62.890	0.686				
3	130.900	0.701				
4	197.310	0.717	0.715	0.997674	6.87	0.2077
5	295.200	0.732	0.734	0.996871	7.01	0.2077
6	364.700	0.747	0.747	0.996669	7.14	0.2268
7	437.550	0.763	0.763	0.999385	7.29	0.2636
8	494.560	0.778	0.780	0.995224	7.44	0.2692
9	540.920	0.794	0.793	0.995482	7.60	0.2850
10	583.980	0.809	0.806	0.994924	7.75	0.3050
11	655.150	0.824	0.827	0.992771	7.90	0.3430
12	694.930	0.840	0.840	0.996616	8.08	0.3848
13	732.150	0.855	0.855	0.998335	8.24	0.4267
14	762.350	0.870	0.870	0.999692	8.41	0.4566
15	796.970	0.886	0.886	0.998751	8.60	0.4922
16	827.390	0.901	0.900	0.994687	8.78	0.5601
17	859.590	0.916	0.919	0.996333	8.97	0.6653
18	881.720	0.932	0.934	0.996736	9.18	0.7309
19	895.920	0.947	0.944	0.996564	9.38	0.8003
20	915.310	0.962	0.961	0.994146	9.59	0.9342
21	936.360	0.978	0.981	0.994416	9.83	1.1086
22	948.250	0.993	0.994	0.997986	10.05	1.2980
23	957.420	1.008	1.006	0.998281	10.29	1.5081
24	969.610	1.024	1.026	0.998222	10.55	1.7922
25	977.270	1.039	1.040	0.998396	10.80	1.9467
26	984.100	1.055	1.053	0.998052	11.09	2.1957
27	991.100	1.070	1.070	0.994795	11.36	2.6015
28	998.080	1.085	1.089	0.994355	11.65	2.8383
29	1002.460	1.101	1.101	0.989753	11.97	3.3258
30	1005.730	1.116	1.112	0.985035	12.29	3.8936
31	1011.990	1.131	1.140	0.965190	12.62	5.8604
32	1013.500	1.147	1.148	0.957489	12.99	8.9414
33	1015.790	1.162	1.173	0.965854	13.36	15.3051
34	1016.340	1.177	1.179	0.975386	13.74	23.2226
35	1016.990	1.193	1.195	0.994033	14.17	34.6124
36	1017.400	1.208	1.209	0.987784	14.59	46.3438
37	1017.790	1.223	1.229	0.976911	15.04	69.9567
38	1017.980	1.239	1.242	0.985736	15.54	98.4429
39	1018.150	1.255	1.259	0.994410	16.07	126.8556
40	1018.200	1.270	1.265	0.990770	16.59	142.2361
41	1018.340	1.286	1.288	0.948474	17.18	217.2128
42	1018.440	1.301				
43	1018.480	1.316				
44	1018.510	1.345				

*-data violates specimen size requirements

Paris exponent 7.607

log of intercept -13.362

Paris coefficient $4.348*10^{-}$ -14.000

A357-T6, L2

Copy available to DTIC does not permit fully legible reproduction

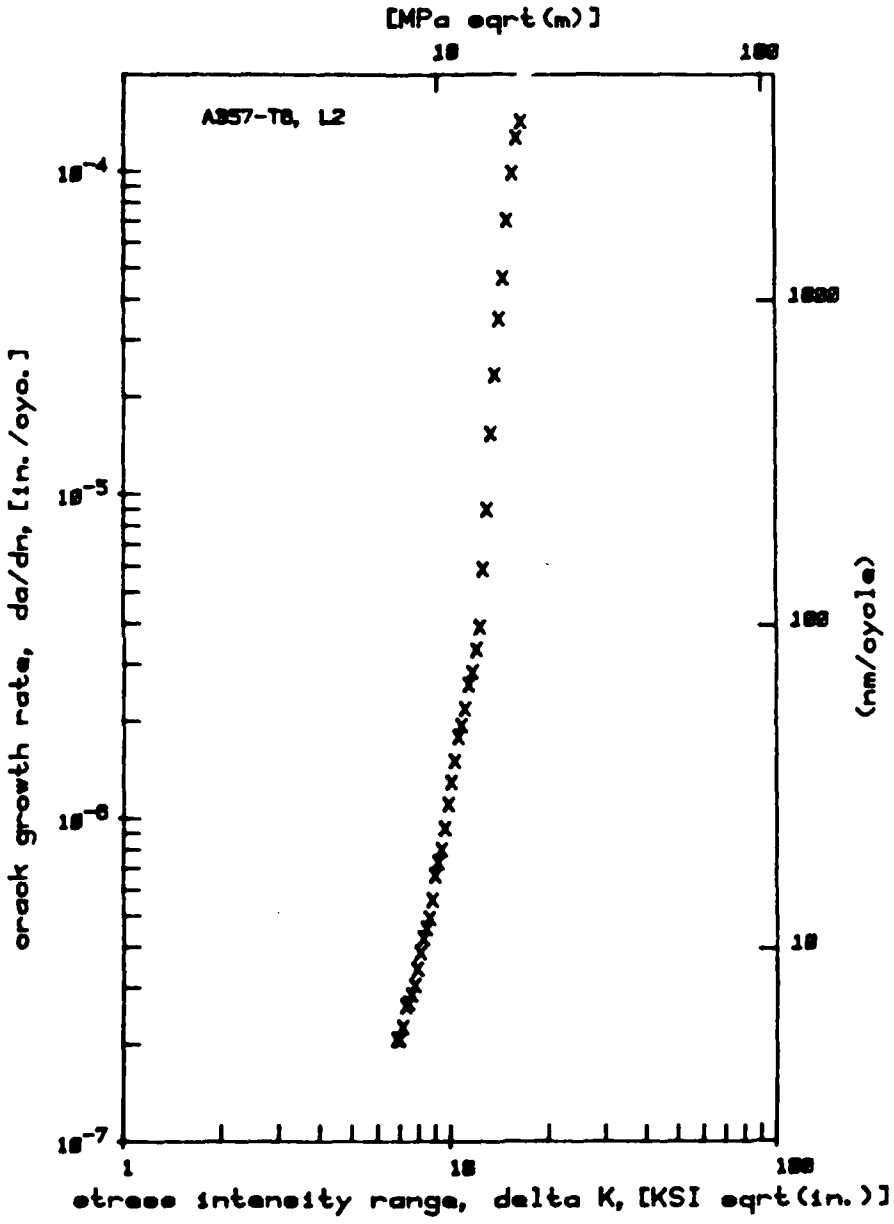
[MPa sqrt(m)]
10
100
A357-T6, L2
10^{-4}
10^{-5}
10^{-6}
10^{-7}
1000
100
10
(nm/cycle)
crack growth rate, da/dn, [in./cyc.]
1
10
100
stress intensity range, delta K, [KSI sqrt(in.)]

8 May 1985

SPECIMEN NO. L3

Pmax = 225 LBF Pmin = 45 LBF P = 0.200

B=0.120 in. W=1.991 in. Crack Correction +0.000 in.

PT #	CYCLE COUNT	A-cor in	A-eq in	MC	delta K ksi√in	da/dN in/cy
1	0.001	0.666				
2	63.050	0.682				
3	133.450	0.697				
4	198.020	0.712	0.712	0.999153	6.93	0.2281
5	273.470	0.728	0.729	0.998912	7.07	0.2308
6	327.350	0.743	0.741	0.998237	7.21	0.2413
7	403.850	0.758	0.759	0.997614	7.36	0.2691
8	459.840	0.774	0.775	0.998200	7.51	0.2996
9	508.400	0.789	0.790	0.995010	7.66	0.3024
10	547.270	0.804	0.803	0.997787	7.82	0.3138
11	592.980	0.820	0.818	0.998005	7.99	0.3167
12	653.130	0.835	0.836	0.995923	8.15	0.3214
13	702.930	0.850	0.851	0.998099	8.32	0.3386
14	748.870	0.866	0.866	0.999663	8.50	0.3731
15	782.960	0.881	0.880	0.999571	8.68	0.3994
16	824.790	0.897	0.897	0.999455	8.88	0.4382
17	856.330	0.912	0.911	0.998381	9.07	0.4828
18	890.690	0.927	0.928	0.996402	9.27	0.5751
19	918.930	0.943	0.944	0.995679	9.49	0.7244
20	940.130	0.958	0.960	0.998028	9.70	0.8384
21	954.440	0.973	0.972	0.997907	9.92	0.9191
22	968.720	0.989	0.987	0.984819	10.17	1.1111
23	986.300	1.004	1.007	0.977341	10.40	1.4734
24	999.020	1.019	1.027	0.982605	10.65	2.0520
25	1001.500	1.035	1.031	0.987309	10.93	2.1182
26	1008.720	1.050	1.048	0.987873	11.20	2.3922
27	1014.450	1.065	1.064	0.991414	11.48	2.6477
28	1021.640	1.081	1.082	0.998543	11.79	2.8121
29	1026.930	1.096	1.097	0.993948	12.10	3.4220
30	1031.700	1.112	1.113	0.995217	12.44	4.3729
31	1035.480	1.127	1.130	0.995605	12.78	5.7468
32	1037.370	1.142	1.141	0.998123	13.13	6.5744
33	1039.960	1.158	1.159	0.998268	13.53	7.7453
34	1041.470	1.173	1.172	0.996980	13.92	8.7908
35	1043.400	1.188	1.189	0.997734	14.33	10.2926
36	1045.020	1.204	1.206	0.983916	14.79	13.7053
37	1046.010	1.219	1.221	0.962921	15.24	19.4746
38	1047.120	1.234	1.248	0.941935	15.72	33.8810
39	1047.340	1.250	1.256	0.944636	16.26	58.2848
40	1047.520	1.265	1.264	0.991056	16.79	79.4461
41	1047.710	1.280	1.282	0.993868	17.36	91.8324
42	1047.820	1.296	1.292	0.981358	18.00	105.3118
43	1048.060	1.312	1.322	0.914458	18.67	185.3851
44	1048.140	1.327				
45	1048.190	1.343				
46	1048.210	1.372				

*-data violates specimen size requirements

Paris exponent 6.710

log of intercept -12.585

Paris coefficient [illegible]*10^ -13.000

A357-T6, L3

Copy available to DTIC does not permit fully legible reproduction

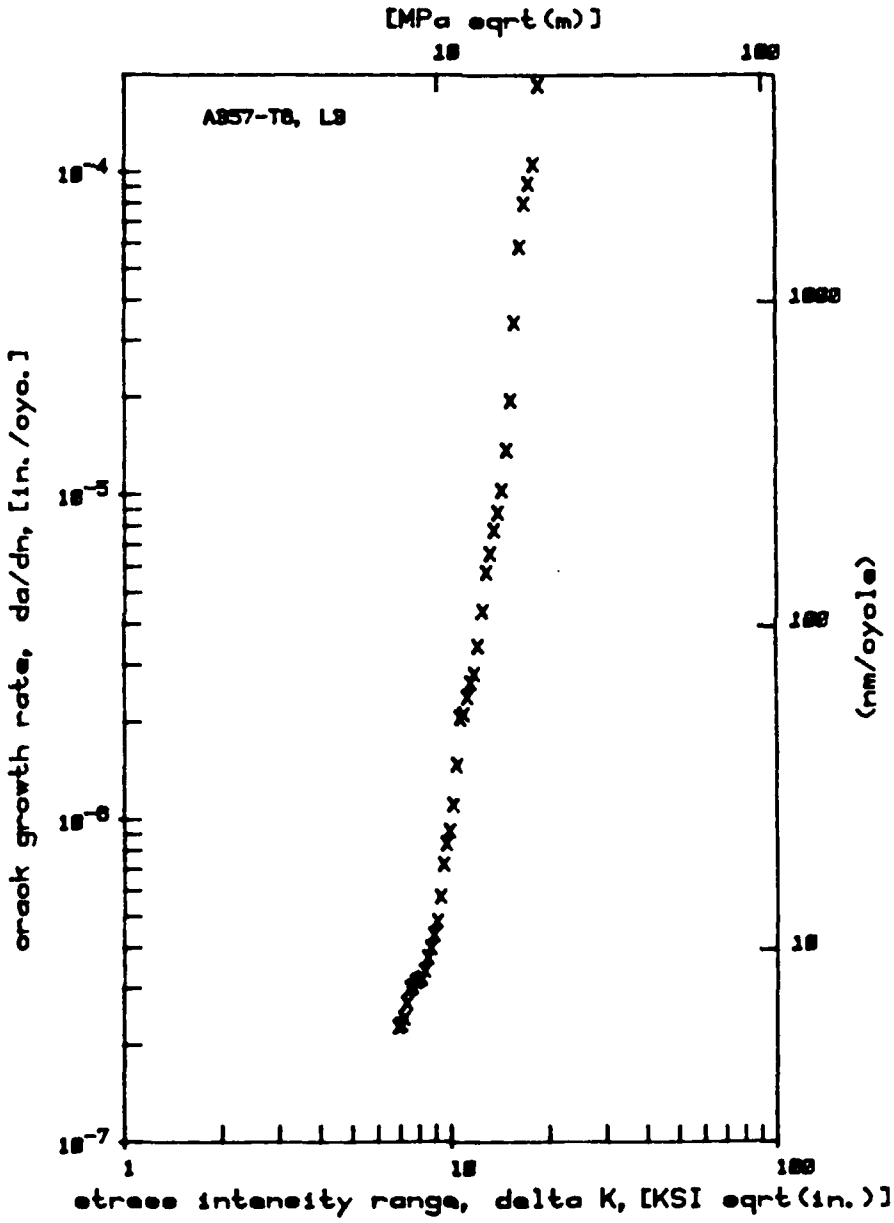
[MPa sqrt(m)]
10
100
A357-T6, L3
10^{-4}
10^{-5}
10^{-6}
10^{-7}
1000
100
10
(nm/cycle)
crack growth rate, da/dn, [in./cyc.]
1
10
100
stress intensity range, delta K, [KSI sqrt(in.)]

BIBLIOGRAPHY

1. Anonymous, "Aluminum Alloys Can Substantially Reduce Aircraft Construction Costs," Aircraft Engineering, Vol 54, No 4, Issue 638, 1982, pp 16-17.

2. Anonymous, "Industry Observer", Aviation Week and Space Technology, 19 September 1983, p 11.

3. B. M. Elson, "Dispenser Modified for Air-Launched Cruise Missile", Aviation Week and Space Technology, 2 April 1979, pp 66-67.

4. Anonymous, "Alcoa Pushes Sand Casting Techniques", Aviation Week and Space Technology, 2 January 1984, pp 49-50.

5. K. J. Oswalt and C. Ford, "Manufacturing Methods for Process Effects on Aluminum Casting Allowables", Air Force Wright Aeronautical Laboratories (AFWAL), Materials Laboratory Contract F33615-79-C-5116, Report Number IR 268-9(I), May 1981, p 1.

6. W.J. Shaw and I. LeMay, "Fatigue Crack Growth Prediction and Intrinsic Material Scatter," Presented at the Symposium on Statistical Analysis of Fatigue Data, American Society for Testing and Materials, Pittsburgh, PA, October 1979.

7. A. P. Berens, J. P. Gallagher and P. W. Hovey, "Statistics of Crack Growth", Structural Reliability and Damage Assessment Symposium of the Ninth U.S. National Congress of Applied Mechanics, 21-25 June 1982.

8. D. A. Virkler, B. N. Hillberry, P. K. Goel, "The Statistical Nature of Fatigue Crack Propagation," Air Force of Scientific Research Contract AFOSR-76-3018, Report Number AFFDL-TR-78-43, April 1978.

9. A. P. Berens, Private Communication, August 1985

10. J. W. Faber, "Cast Aluminum Structures Technology (CAST), Technology Transfer (Phase VI) Summary Technical Report," AFWAL Flight Dynamics Laboratory Contract F33615-76-C-3111, Report Number AFWAL-TR-80-3020, April 1980.

11. D. L. McLellan and M. M. Tuttle, "Manufacturing Methodology Improvement for Aluminum Casting Ductility," AFWAL Materials Laboratory Contract F33615-80-C-3209, Report Number AFWAL-TR-82-4135, December 1982.

12. "Cast Aluminum Structures Technology (CAST), Technical Bulletin No. 6, Portable Metallographic Technique for Determination of Dendrite Arm Spacing (DAS) on Castings," AFWAL Materials Laboratory Contract F33615-76-C-3111, June 1978, p.8.

13. R. R. Cervay, "Automated Fatigue Crack Growth Data Acquisition System Evaluation," University of Dayton Research Institute (UDRI), Report Number UDR-TM-84-42, November 1984.

14. H. S. Pearson and G. J. Gilbert, "Automated Crack Growth Testing - Evaluation of a Bonded Foil Crack-Gage System," American Society for Testing and Materials (ASTM) Spring Meeting of Committee E-24 on Fracture Testing of Metals, 16-20 March 1981.

15. ASTM Standard E647-83 Standard Test Method for Constant-Load-Amplitude Fatigue Crack Growth Rates above 10^{-8} m/cycle, Vol 03.01, 1983.

16. ASTM Standard B557-81 Standard Methods of Tension Testing Wrought and Cast Aluminum and Magnesium Alloy Products, ASTM Book of Standards Vol 03.01, 1983.

17. J. D. Tirpak, "Fatigue Crack Growth Testing of Cast Aluminum Alloy A357-T6," AFWAL Materials Laboratory In-House, Report Number MLS-84-37, April 1984.

18. J. D. Tirpak, Y. Kim, D. Eylon, Unpublished work 1983.

19. J. Leupp, "The Fracture Characteristics of Aluminum Cast Alloys", Material und Technik, No. 1., 1983, pp 5-10.

20. R. J. Stofanak, R. W. Hertzberg, J. Leupp, and R. Jaccards, "On the Cyclic Behavior of Cast and Extruded Aluminum Alloys, Part B: Fractography," Engineering Fracture Mechanics, Vol 17, No 6, 1983, pp 541-554.

U.S. Government Printing Office: 1986 748 061/60537